

Revisiting Granular Models of Firm Growth⁰

José Moran^{1,2,3}, Angelo Secchi⁴, and Jean-Philippe Bouchaud^{5,6,7}

¹Macrocosm Inc., Brooklyn NY 1 242 120

²Institute for New Economic Thinking at the Oxford Martin School, University of Oxford 79 82 7

³Complexity Science Hub, Vienna 242 120 22

⁴PSE - Université Paris 1 Panthéon-Sorbonne 242 120 22

⁵Capital Fund Management, Paris 242 120 22

⁶Chair of Econophysics and Complex Systems, École Polytechnique 136 79 16

⁷Académie des Sciences, Paris 22 33 45

June 9, 2024 22 33 45

Abstract

We revisit the “granular models of firm growth” that have been proposed in the literature over 2
the past two decades to explain the anomalously slow decrease of growth volatility with firms size 2
and how this phenomenon shapes the distribution of their growth rates. In these models, firms’ sales 2
are viewed as collections of independent “sub-units”, and these non-trivial statistical properties 2
occur as a direct result of the fat-tailed distribution of the number or sizes of these sub-units. 2

In revisiting these models we present and discuss new theoretical results on the relation between 2
firm size and growth rate statistics. Our results can be understood intuitively by noting that 2
granular models imply the existence of three types of firms: well-diversified firms, with a size evenly 2
distributed among several sub-units; firms with many sub-units but with their total size concentrated 2
on only a handful of them, and lastly firms which are poorly diversified simply because they are 2
made up of a small number of sub-units. 2

Inspired by our theoretical insights, we establish new empirical facts about growth rates and 2
their relation with size. As predicted by the model, the distribution of growth rate volatilities is 2
to a good approximation independent of firm size, once rescaled by the average size-conditioned 2
volatility. However, the tail of this distribution is *much too thin* to be consistent with a granular 2
mechanism. Moreover, the moments of growth volatility conditional on size scale with size in a way 2
that is unambiguously at odds with theoretical predictions. We also find that the distribution of 2
growth rates rescaled by firm-specific volatility, which is predicted to be Gaussian by all the models 2
we consider, remains very fat-tailed in the data, even for large firms. This paper, in ruling out the 2
granularity scenario, suggests that the overarching mechanisms underlying the growth of firms are 2
not satisfactorily understood, and argues that they deserve further theoretical investigations. 2

1. Introduction 3

What statistical laws does the growth of firms abide to? The growth dynamics of firms depends of course on a host of both common and idiosyncratic time-dependent factors and hence a purely statistical approach to this question might appear somewhat futile. Still the research of the past three decades has made it increasingly evident that changes in macro aggregates like GDP are best understood in light of the statistics of business activities at the firm level (Haltiwanger, 1997). Moreover, the questions raised by company growth statistics are deeply related not only to macroeconomic fluctuations, but also to the growth of individual wealth or the growth of city sizes, topics that have also received a large amount of attention in an interdisciplinary literature (Gabaix, 2009). Further to this, and in spite of emerging from very heterogeneous statistical samples, many statistical facts pertaining to firm growth have been shown to be robust and to some extent universal, in that they hold across different countries, time periods and levels of aggregation, and in that they do so independently of the size proxy that is used (Buldyrev et al., 2020; Dosi, 2023).⁴

Among the best known statistical properties of firm growth is the fact that both the firm size distribution and the growth rate distribution are non-Gaussian (Axtell, 2001; Stanley et al., 1996) and feature heavy tails. As a forceful illustration of the latter, we represent in Figure 1 (left-panel, purple line) the empirical density of year-on-year sales growth rates computed over a large sample of publicly traded companies in the United States.¹ As is well documented in the literature, the distribution is to a large extent symmetric, which in itself is somewhat unexpected, and features a “cusp” in the central part along with slowly decaying tails. This implies relatively frequent episodes of extreme growth or extreme decline: the probability to observe sales multiplied or divided by more than 150 is as large as one in one thousand, an event nearly impossible if the growth rates follow a Gaussian distribution.⁵

However, characterizing this distribution when the growth rates of different firms are pooled together is clearly not a neutral choice. Implicitly, it assumes that all the observations are drawn from the same, firm-independent and time-independent distribution. This is clearly unreasonable, in particular with regard to another well-known statistical property, first established by Hymer and Pashigian (1962), suggesting a decline of growth volatility with size that looks inconsistent with a simple diversification argument. In the mid-nineties, thanks to the availability of comprehensive balance-sheet data, Stanley et al. (1996) and Amaral et al. (1997) provided a quantitatively accurate characterization of this scaling relation. The standard deviation of growth rates is shown to decrease with a firm’s size S_i as a power-law $S_i^{-\beta}$, where β is found approximately equal to 0.2.² This decay is significantly slower than the one a simple diversification argument would suggest, which would correspond to $\beta = 0.5$.⁶

This paper addresses the question of explaining the emergence of these two empirical laws. We consider a concise market economy comprising firms with exogenous production and operating in independent markets. Because of the lack of direct competition among firms, these models are known as “island models” (Sutton, 1997). In this framework, reminiscent of the one introduced by Gibrat (1931) to explain the firm size distribution, a firm’s size evolves according to a multiplicative process, modeling its growth rate as a random variable.⁷

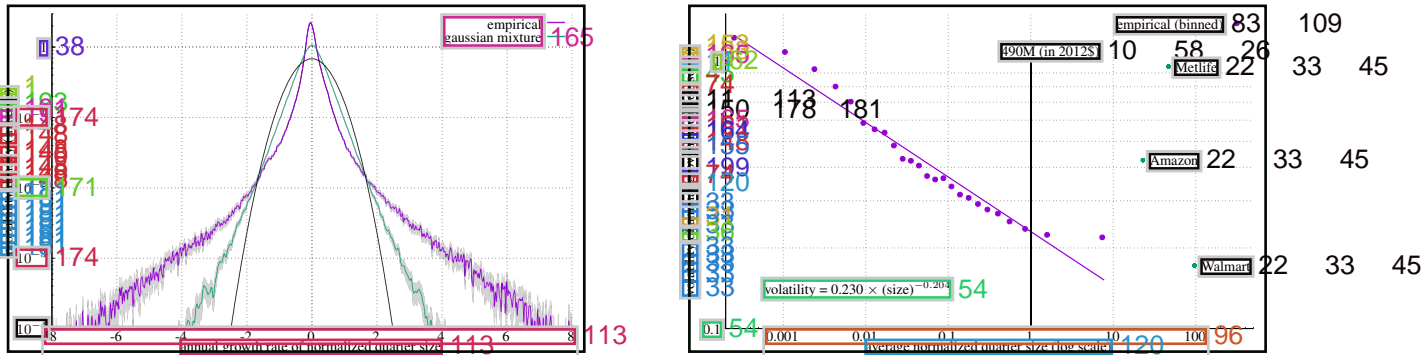
The simplest idea to explain the two empirical laws under scrutiny would then be to assume that idiosyncratic growth shocks are Gaussian, but with a firm-dependent volatility σ_i that only depends on the size S_i of firm i as in $\sigma_i = \sigma_0 S_i^{-\rho}$.⁸ This is equivalent to saying that a firm’s growth volatility is uniquely determined by its size, and imposing a black-box type relation on the many reasons explaining why larger firms, possibly because of diversification, have less volatile growth. The resulting distribution of growth rates can be seen as a *Gaussian mixture*, as it is the superposition of Gaussian distributions with heterogeneous variances. The family of “scale mixtures of Gaussian distributions” is known to have generically fatter tails than a Gaussian distribution, and it is versatile enough to generate a wide class of continuous, unimodal and symmetric distributions (West, 1987; Andrews and Mallows, 1974).⁹

¹This figure uses data on publicly traded US companies drawn from COMPUSTAT. Details on the data are reported in Section 3.1 and in the Notes under the figure.¹⁰

²Interestingly, and in spite of being a quantity that does not *a priori* follow the same dynamics as firm sales, one finds the same dependence of the volatility of the returns of traded stocks as a function of their market capitalisation. Such a coincidence was also noted by Herskovic et al. (2020).¹¹

³Among the distributions that can be represented as Gaussian mixtures, one finds the Student-*t*, Logistic, Laplace,

Figure 1: Distribution of the annual growth rate and its size dependent volatility 79 82 12



Notes: Left-panel reports the kernel estimate of the unconditional empirical density of the growth rates after removing the mean (purple line). The estimate is computed using the entire sample pooling annual (log) growth rates across firms and year-quarter with a Gaussian kernel function and a bandwidth chosen according to the normal reference rule-of-thumb. The estimate is evaluated on a 10,000 points regular grid defined over the entire empirical range. We also report the 95% confidence interval and the Gaussian parametric fit (dotted line). We add the empirical density of synthetic growth rates (green line) obtained by mixing Gaussian random shocks with growth volatilities bootstrapped from those estimated according to $\sigma(S) \propto S^{-\beta}$, as suggested by the right panel, and a Normal fit (black line). Right-panel displays on a double log-scale the binned relation between firms' growth volatility and average normalized size. Each point represents the average size and the average volatility of the growth rates of firms belonging to the same size bin where volatility is proxied with the mean absolute deviation adjusted by the factor $\sqrt{\pi/2}$. We also report a power-law fit $\sigma(S) \propto S^{-\beta}$ where the exponent β is found approximately equal to -0.204 with an asymptotic standard error of 0.01 . Note however that the rightmost part of the data decays even more slowly. Data source: Compustat.

Unfortunately, as is illustrated in Figure 1, this simple reasoning still falls short of explaining the empirical distribution of growth rates: although the resulting Gaussian mixture is indeed heavy tailed (dark-green line), as seen from comparing it with the Gaussian benchmark (black line), it misses its empirical target (purple line). In addition to this, the right panel of the same figure shows that although the volatility-size scaling relation holds in a wide range, it does not describe the volatility of very large corporations very well.⁴ A more careful analysis of the data also suggests important fluctuations around the average value of growth volatility conditional on size.⁹

To overcome this problem, the literature has considered the possibility that firms with similar size may have additional sources of variability of their growth trajectories. A simple way to obtain this result is to enrich basic island models with two intertwined features. The first is that firms can operate in more than one market. As a consequence, each firm can be seen as an ensemble of sub-units, with each functioning in one of these distinct and independent markets. The second is that these sub-units may not necessarily be of equal size, so that a firm's aggregate size can be concentrated in only a "granular" handful of them. Sutton (2002), Fu et al. (2005), Buldyrev et al. (2007) and Schwarzkopf et al. (2010) provide examples of growth models adopting this strategy. While these *compositional models* all share the feature that the distribution of growth rates they generate is a Gaussian mixture that can reproduce the shape of the empirical distribution quite well they fail in capturing the size-volatility relation (Moran and Riccaboni, 2024). Among the same family, two notable exceptions are presented in Wyart and Bouchaud (2003) and Gabaix (2011).⁵ Their two models are indeed able to accommodate the slow decay of growth volatilities with size and the non-Gaussian distribution of growth rates allowing for the so-called "granular" effects. For this reason, we name them "granular models of firm growth", and they represent the key antecedents with respect to which the present work makes its main contributions.⁶

Lévy-stable and Power-exponential distributions, all of which have been considered as good candidates to describe the empirical distribution of growth rates.⁸

⁴Evidence pointing in the same direction has been found for French firms in Fontanelli et al. (2024).

⁵Another exception would be Sutton (2002). The model presented therein leads to an average growth volatility conditional on size that scales with an exponent equal to $1/4$, close to the empirical value 0.2 . However, the model is developed assuming that all partitions of a firm's size into sub-units are equiprobable (microcanonical hypothesis), an hypothesis difficult to justify in our context, see also the discussion in Wyart and Bouchaud (2003).¹⁰

⁶For a version of the model where "granularity" comes from supplier-customer network effects, see Herskovic et al. (2020).¹¹

We propose a unified theoretical framework in which Gabaix (2011) and Wyart and Bouchaud (2003) only differ through the assumptions they make on the statistics of the number of sub-units composing each firm: a number that is roughly proportional to the firm's size in the first case, and a random variable with a skewed distribution for the latter. We refine the analyses of the two models and provide formal proofs to some of the conjectures they raised, while also correcting some of their results. In particular, we show that growth volatility is not only driven by firm size but by a more complicated interplay between a firm's size and its structure. This is explained by showing that these models imply the existence of three different types of firms: those with sales evenly distributed among a large number of sub-units, those with a large number of sub-units but with their sales concentrated only on a few of them, and lastly those made up of only a handful of sub-units. Such a description, in spite of being well adapted to the description of large firms, paints very different pictures of how well diversified they are, an issue also raised in the international trade literature by Kramarz et al. (2020). We show that the co-existence of these three types of firms has a direct impact on the shape of the growth volatility distribution and we derive non-trivial results on the scaling laws of its first four moments. This allows us to discuss in details the distribution of the growth rates predicted by the model since in this framework it simply results from mixing Gaussian random variables using the volatility distribution as a mixing function. 12

In addition to these theoretical results, we provide a twofold empirical contribution. Our first contribution is the determination of new empirical facts about the growth dynamics of business firms. Guided by the theoretical considerations above, we show that the distribution of the growth rate volatility, once rescaled by its average conditional on size, is to a good approximation independent of firm size, and is well approximated by an Inverse Gamma distribution, which features a power-law right tail. We also document that the first four moments of growth volatility, and not only the average, scale down with size as a power-law. Our second contribution is to show that although these observations are to a first approximation in good qualitative agreement with granular models of growth, a deeper investigation unveils three major inconsistencies. The first of these is that the tail of the empirical distribution of the growth volatility is much too thin to be compatible with the tail a granular model would predict. This means that we do not observe large volatilities in the data as often as predicted by a calibrated granular model. The second empirical inconsistency is that moments higher than order one do not all decrease with size at the same scaling rate, at odds with what the model predicts. Finally, the last inconsistency is that the two granular models we have analyzed imply that a firm's growth rate, when rescaled by the firm-dependent volatility, should be distributed as a Gaussian random variable. We expect this to be true in particular for large firms: since in the two models their growth rates are the sum of a large number of (possibly non-Gaussian) independent random variables, the Central Limit Theorem predicts that they should be partially Gaussian. However, their empirical distribution deviates from a Gaussian benchmark, and we quantify this deviation by proposing a generic family of distributions that features a Gaussian central region of varying width and exponentially "stretched" tails. Somewhat surprisingly, parametric fits of these distributions show that the tails do not gradually disappear when considering larger firms, even though they do (at a slow rate) when considering longer time horizons in building growth rates. 13

Putting it all together, our analysis shows that compositional growth models, and in particular the granular growth models analyzed in this paper, are not able to account for the rich statistical features characterizing the growth of business firms. This ultimately suggests that the overarching mechanisms driving their evolution are not yet satisfactorily understood. Possible mechanisms to alleviate this are suggested in the concluding section. 14

2. Modeling firm growth: a rigorous statistical approach 15

In this section, we present a statistical framework to describe the dynamics of firms' growth and how they are modulated by their size. Our primary objective is to investigate the extent to which this framework is compatible with the two empirical facts motivating this paper, namely (i) the non-Gaussian shape of the growth rates distribution and (ii) the slow decay with size of the volatility

of firms growth rates. After defining the basic set-up, we consider two instances of the statistical framework featuring one and two sources of granularity so revisiting the models presented in Gabaix (2011) and Wyart and Bouchaud (2003) respectively. We refine their analyses and correct some of their results, deriving new and more precise predictions that can be directly compared with data. 16

2.1. Set-up 17

We analyze a concise market economy comprising N firms, which are characterized by an exogenous production. We posit that each sufficiently large firm consists of a specific number of sub-units, which can be construed as departments or production units, each of which functions within distinct and independent sub-markets. These units might alternatively thought of as representing lines of business with different customers, in the spirit of Herskovic et al. (2020). 18

The size of firm i at time t is denoted by S_{it} and satisfies $S_{it} = \sum_{j=1}^{K_i} s_{jit}$, where K_i represents the number of sub-units and $s_{ jit}, j = 1, \dots, K_i$, denotes their respective sizes. The evolution of each sub-unit's size over time is assumed to follow a multiplicative process with growth rates of finite variance. This definition becomes the following assumption. 19

Assumption 1. *The time evolution of each sub-unit's size is characterized by a multiplicative process* 20

$$s_{ jit+1} = (1 + \sigma_0 \eta_{ jit}) s_{ jit} , \quad (1) \quad 20$$

where $\eta_{ jit}$ are independent random shocks with zero mean and unit variance. The time invariant parameter σ_0 defines the order of magnitude of the growth fluctuations at the level of a sub-unit. For definiteness, the unit of t is given in years. 20

Assumption 1 implies that the absolute growth of each sub-unit is proportional to its size, something known in the litterature as the “Law of Proportionate Effects” or “Gibrat’s Law”. The assumption that all the sub-unit shocks $\eta_{ ji}$ have a standard deviation σ_0 that is independent of i and j is a simplification needed to make the model analytically tractable.⁷ Using Equation (1), we can then write a firm's year-on-year growth rate as 21

$$g_{ it} := \frac{S_{ it+1} - S_{ it}}{S_{ it}} = \frac{1}{S_{ it}} \sum_{j=1}^{K_i} s_{ jit} \eta_{ jit} . \quad (2) \quad 33$$

Within this framework, one could further assume that all the sub-unit are of approximately the same size, say \bar{s}_i . In this case, a firm's size and its number of sub-units would be directly proportional, that is $S_i \approx K_i \bar{s}_i$. A direct application of the Central Limit Theorem implies that for large firms, and therefore firms with a large number of sub-units, the growth rates g_i are well described by a Gaussian distribution with a standard deviation of $\sigma_0 S_i^{-\beta}$ with $\beta = 1/2$. Thus, larger firms would appear less volatile than smaller firms because they have a higher number of sub-units, and are therefore better diversified. 23

This conclusion is, however, at odds with empirical observations, which note that growth rates are markedly non-Gaussian, even when large firms are studied. Further, the decay in volatility with respect to firm size is much slower than in the anticipated $\sigma_0 S_i^{-1/2}$, meaning that large firms are more volatile than one would anticipate if all sub-unit sizes were approximately equal. In the remaining of this section, we investigate the inadequacy of this model in explaining the observed phenomena by considering two versions of our statistical framework. The first one, due to Gabaix (2011), features a single source of granularity, namely the size distribution of the sub-units composing a firm. The second, due to Wyart and Bouchaud (2003), adds another source of granularity through the distribution of the number of such sub-units. 24

⁷Note that heterogeneous volatilities can be resorbed into the definition of $s_{ ij} \rightarrow \sigma_{ ij} s_{ ij}$. The discussion on firm size statistics still depends on the distribution of $s_{ ij}$ alone, but growth rate statistics can be understood using the same theoretical machinery by considering the variable $\sigma_{ ij} s_{ ij}$ rather than $s_{ ij}$ alone. 21

2.2. Single granularity hypothesis [Gabaix' model] 22

In this section, we depart from the assumption that sub-units are characterized by relatively similar sizes s_{ji} by positing that the firms size distribution features a heavy tail following the idea proposed in Gabaix (2011).⁸ In line with the original model, we assume the following. 26

Assumption 2. The size of a sub-unit s_{ji} is a random variable assumed to be larger than a lower bound s_0 , representing the minimal size of a sub-unit. Its distribution is Pareto over the interval $[s_0; \infty)$. 27

$$P(s_{ji}) = \frac{\mu}{s_0} \left(\frac{s_{ji}}{s_0} \right)^{-(1+\mu)} \quad s_0 > 0, \quad 1 < \mu < 2 . \quad 22$$

The distribution $P(s_{ji})$ is taken to be time-invariant. Note that since $\mu > 1$, the average sub-unit size $\mathbb{E}[s_i] := \bar{s}_i$ exists and is finite. 48

To stay close to Gabaix's original model, where no explicit assumption is made on the statistics of sub-units number K_i , we assume that K_i is close to S_i/\bar{s}_i for large firms. 28

Assumption 3. For firms of size $S \gg \bar{s}$ and for $\mu > 1$, the number of sub-units K is given by⁹ 99

$$K = \frac{S}{\bar{s}} \quad 159(S) \quad 60$$

In our revisiting of Gabaix' model, we first discuss the relation between a firm's size and the Herfindahl-Hirschman index (HHI) measuring its concentration of sales among sub-units. We shall then study the distribution of the growth rate volatility conditional on size, and how its shape ultimately determines that of the growth rates when we pool together heterogeneous firms. 30

Variance of growth rates. Now, since we assume that sub-units fluctuate independently, the variance of the growth rate of firm i , denoted as σ_i^2 , is given by 32

$$\sigma_i^2 = \sigma_0^2 \frac{\sum_{j=1}^K s_{ji}^2}{(\sum_{j=1}^K s_{ji})^2} := \sigma_0^2 \mathcal{H} , \quad (3) \quad 31$$

where \mathcal{H} represents the Herfindahl-Hirschman index (HHI) of the sub-unit sizes of firm i . As noted by Gabaix, equation (3) states that the variance of the growth rates is proportional to an index measuring the concentration of a firm's sales across its different sub-units. 34

Anomalous scaling behavior of \mathcal{H} . The core result in Gabaix (2011) can now be restated in our framework by saying that when $1 < \mu < 2$ and $K \rightarrow \infty$, the typical value (i.e. the modal value) of the Herfindahl-Hirschman index behaves as $\mathcal{H}_{typ} \sim \mathcal{O}(K^{2(1-\mu)/\mu})$.¹⁰ An implication of this is that \mathcal{H}_{typ} decays to 0 much slower than what one would get in the case where $\mu > 2$, where \mathcal{H}_{typ} would behave as $\mathcal{O}(K^{-1})$. This last case leads to a growth rate volatility that is proportional to the square root of the HHI, $\sigma \propto \sqrt{\mathcal{H}}$, and therefore to the scaling $S^{-1/2}$ described above. Hence, in this granular setting diversification is not as effective, since the existence of particularly large and "granular" entities impedes the standard diversification argument with a scaling in $S^{-1/2}$ and gives instead the slow decay of the Herfindahl-Hirschman index described above.¹¹ 36

⁸Originally this granularity scenario was proposed to explain the anomalously large fluctuations of GDP in economies populated by firms whose size could be extremely large. Here we reinterpret a firm in the original paper as a sub-unit and a country as a firm. The remaining argument remains the same. 126

⁹More precisely $(\sum_{j=1}^K s_{ji} - K\bar{s}_i)/K^{1/\mu}$ converges for large K to a Lévy-stable random variable, see Gnedenko and Kolmogorov (1953). This means that the typical fluctuations of $\sum_{j=1}^K s_{ji} - S$ are of order $K^{1/\mu}$. Since S and K are asymptotically proportional, this implies that the fluctuations of S are of order $S^{1/\mu}$, and thus negligible except when $\mu < 1$. 29

¹⁰See Proposition 1 in Appendix A which replicates Proposition 2 pp. 740 in Gabaix (2011) after noting that $\sigma = \sqrt{\mathcal{H}}$ and that S is proportional to K . Throughout this paper, as in the original work, the symbol \approx means approximately equal to, the symbol \sim means that the ratio of between the left- and right-hand side terms tends to a positive real number as the argument tends to infinite. This can be considered as an asymptotic version of the \propto symbol, representing proportionality between two terms. 135

¹¹To complete the cases explored in the original paper, note that $\mathcal{H}_{typ} = \mathcal{O}(1/\ln K)$ when $\mu = 1$. However in this case the assumption that $K = S/\bar{s}$ breaks down. 36

The full study of the case where $1 < \mu < 2$ is in fact more subtle. The problem, overlooked by Gabaix (2011), lies in the fact that the average value of \mathcal{H} is much larger than the typical value, $\mathbb{E}[\mathcal{H}] \gg \mathcal{H}_{typ}$. We obtain this result by extending the approach proposed in Derrida (1997), which we leverage to obtain the asymptotic value of all integer moments $\mathbb{E}[\mathcal{H}^k]$ with $k \in \mathbb{N}$, and to characterize the probability distribution of the Herfindahl-Hirschman index conditional on the number of sub-units, giving the following proposition. 37

Proposition 1. For fixed $K \gg 1$, the distribution of the Herfindahl-Hirschman index takes the following form 38

$$P(\mathcal{H}|K) = K^{2(\mu-1)/\mu} F\left(\mathcal{H}K^{2(\mu-1)/\mu}\right) \left(1 - \sqrt{\mathcal{H}}\right)^{\mu-1}, \quad (4)$$

with $F(x) \sim \frac{1}{x+1}$ 38 when $1 \ll x \lesssim K^{2(\mu-1)/\mu}$. 22 33 45

Proof. See Appendix A.2. ■ 22 33 4

Proposition 1 defines the structure of the conditional distribution of the HHi. The function $F(\cdot)$ is a scaling function that is peaked approximately at $\mathcal{O}(1)$, ensuring that the mode of the distribution $P(\mathcal{H}|K)$ is $\mathcal{H}_{typ} \sim \mathcal{O}(K^{2(1-\mu)/\mu})$. Next, using the distribution in Eq.(4), we can compute the asymptotic behavior of all moments $\mathbb{E}[\mathcal{H}^q|K]$ for any $q > 0$, obtaining the following proposition. 40

Proposition 2. For all $q > 0$, the moments of \mathcal{H} conditional on K are given, to the leading order for $K \gg 1$, by 41

$$\mathbb{E}[\mathcal{H}^q|K] \approx C_1 K^{1-\mu} + C_2 K^{2q\frac{1-\mu}{\mu}} + \mathcal{O}\left(K^{\min(1-\mu, 2q\frac{1-\mu}{\mu})}\right), \quad (5)$$

where C_1 and C_2 are two constants. 41

Proof. See Appendix A.3. ■ 45

This proposition states that the conditional moments of the HHi contain two leading contributions: 43 the first behaving as $K^{1-\mu}$ and the second one as $K^{2q\frac{1-\mu}{\mu}}$ 43 that is as \mathcal{H}^q . 43 The former is dominant 43 whenever $1 - \mu > 2q\frac{1-\mu}{\mu}$ 43, i.e. $q > \mu/2$, while the latter is dominant when $q < \mu/2$. 43

Since we work under the assumption that $1 < \mu < 2$, the first term in Eq. (5) is dominant for 44 $q = 1$, showing that $\mathbb{E}[\mathcal{H}|K]$ is larger than its typical value \mathcal{H}_{typ} . When $q = 1/2$, on the contrary, it is 44 the second term that dominates and $\mathbb{E}[\sqrt{\mathcal{H}}|K]$ is driven by the typical value of the HHi. Hence, in 44 summary, we find that 44

$$\sqrt{\mathbb{E}[\mathcal{H}|K]} \sim K^{(1-\mu)/2} \quad \mathbb{E}[\sqrt{\mathcal{H}}|K] \sim K^{(1-\mu)/\mu}. \quad (6)$$

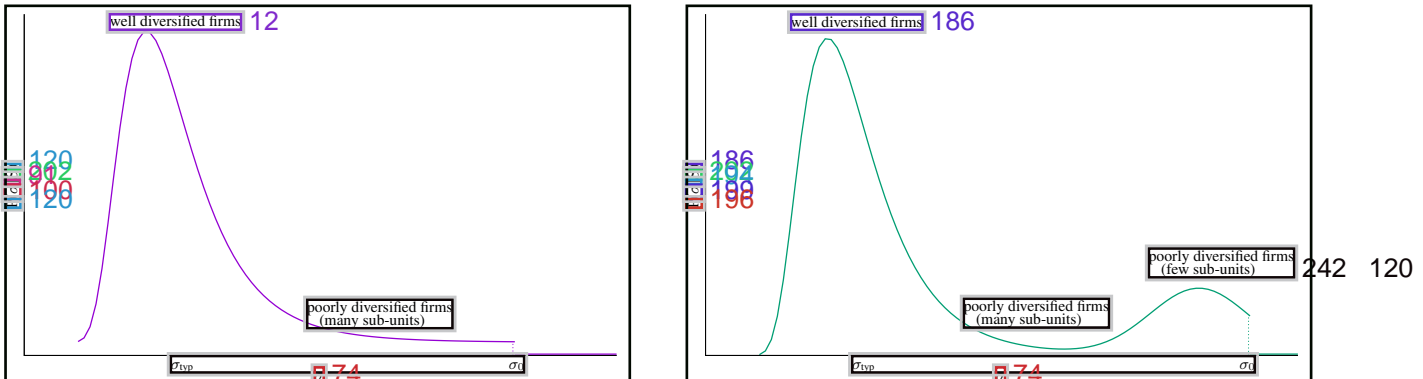
In plain English, this means that the scaling relation one observes is different if one considers the square-root of the average HHi or the average of the square-root of the HHi. The economic interpretation 46 behind this unexpected result is that the model describes a market where two types of large firms 46 coexist. The first type is composed by poorly diversified firms with an abnormally high HHi ($\mathcal{H} \approx 1$), 46 namely firms with one or two dominant sub-units in terms of sales. These high values of the HHi drive 46 the behavior of $\sqrt{\mathbb{E}[\mathcal{H}|K]}$. The second type is composed, on the contrary, by well diversified large 46 firms representing the typical case. These are dominant in driving $\mathbb{E}[\sqrt{\mathcal{H}}|K]$. The existence of the first 46 type of large firms, overlooked in Gabaix (2011), is at the origin of the anomalous scaling exponents. 46 Further it has important consequences on the behavior of the growth volatilities σ_i and ultimately on 46 the shape of the growth rates distribution. Two aspects we investigate below. 46

Conditional distribution of the growth rate volatility. Since the volatility of the growth 47 rate is equal to $\sigma_0 \sqrt{\mathcal{H}}$, and since K and S are proportional ($S \approx K\bar{s}$) all the results concerning the 47 Herfindahl-Hirschman index naturally extend to the growth volatility. The anomalous scaling in Eq. (6) 47 now becomes 47

$$\mathbb{E}[\sigma|S] \approx \sigma_0 \left(\frac{S}{\bar{s}}\right)^{(1-\mu)/\mu} \quad \sqrt{\mathbb{E}[\sigma^2|S]} = \sigma_0 \left(\frac{S}{\bar{s}}\right)^{(1-\mu)/2}, \quad (7)$$

showing again two different values of the exponent in the scaling relation depending on whether one 49 considers the average volatility of growth rates or the square-root of the average squared volatility. 49

Figure 2: Qualitative behavior of $P(\sigma|S)$ 30



Notes: Left-panel reports the qualitative behavior of the distribution of the growth rate volatility $P(\sigma|S)$ with a single granularity source defined in Eq. 8. The bulk of the distribution is constituted by firms that are well diversified with an HHi around σ_{typ} . The power law right tail up to $\sigma \approx \sigma_0$ is generated by poorly diversified firms with a very unequal internal size distribution across sub-units. At σ_0 the power law tail is truncated. Right-panel reports the qualitative behavior of the distribution of the growth rate volatility $P(\sigma|S)$ with two granularity sources in Eq. (10). In this case there is an additional contribution, a peak close to $\mathcal{H} \approx 1$ of relative total weight of order $S^{\alpha-\mu}$, corresponding in that case to large firms that are made up of a very small number of sub-units. In both panel the qualitative behavior has been reproduced using an Inverse Gamma distribution. 54

Similarly, the conditional distribution of volatilities can be deduced from Eq. (4) by substituting $\sigma = \sigma_0 \sqrt{\mathcal{H}}$ to obtain 50

$$P(\sigma|S) = \frac{1}{\bar{\sigma}(S)} G\left(\frac{\sigma}{\bar{\sigma}(S)}\right) \left(1 - \frac{\sigma}{\sigma_0}\right)^{\mu-1}, \quad \text{with } G(x) = 2xF(x^2), \quad (8) \quad 51$$

where $F(\cdot)$ is the same function defined in Eq. 4 above and $\bar{\sigma}(S) := \mathbb{E}[\sigma|S]$ 52

Note that Eq. (8) implies that $P(\sigma|S)$ is a truncated power-law: indeed, $P(\sigma|S) \approx G\left(\frac{\sigma}{\sigma_0}\right)$ when $\sigma \ll \sigma_0$, and therefore $P(\sigma|S) \propto \sigma^{-1-\mu}$ in the regime $\bar{\sigma}(S) \ll \sigma \ll \sigma_0$. This is of course valid up to $\sigma = \sigma_0$, indicating the extreme case where the sales of a firm are concentrated in a single subunit, leading to $P(\sigma_0|S) = 0$ and establishing the cut-off of the power-law. This reflects the two types of firms: those close to the mode which have $\sigma \approx \bar{\sigma}(S)$ and those which are in the tail and are therefore poorly diversified. The entire distribution of the volatilities $P(\sigma) = \int dS P(S)P(\sigma|S)$ can be recovered from this, and will retain the truncated power-law nature of the conditional distributions. A qualitative representation of $P(\sigma|S)$ is reported in Figure 2 (left-panel), highlighting the two types of firms that shape the distribution. 53

2.3. Double granularity hypothesis [Wyart and Bouchaud's model] 48

In this section we extend our statistical framework adding a second source of granularity associated with the number of sub-units following the idea introduced in Wyart and Bouchaud (2003) (WB hereafter). While Assumptions 1 and 2 remain the same, we modify Assumption 3 by stating that the number of sub-units is itself a random variable distributed as a Pareto. Formally, this is stated as follows. 56

Assumption 4. The number of sub-units K_i is random variable assumed to be distributed according to Pareto over the interval $[1; \infty)$. 57

$$P(K_i) = \alpha K_i^{-(1+\alpha)} \quad 45 \quad 1 < \alpha < \mu < 2. \quad 45$$

The distribution $P(K)$ is taken to be time-invariant. 57

Note first that, while the number of sub-units K_i is an integer, we model it as a continuous random variable for mathematical convenience. The results we provide in this section do not depend on the minute details of the distributions of K_i , but only on the behavior of its tail. In the following, we take

Assumption 4 to be true for all of our derivations, which lets us clarify and generalize the results found in Wyart and Bouchaud (2003).⁵⁸ 58

Firm size distribution. We start our analysis by focusing on the firm size distribution, an aspect that could not be investigated within the single granularity set-up because of the lack of a specific assumption on $P(K_i)$. The behavior of the firm size distribution in a model with granularity both in the size and number of sub-units is presented in the following proposition.⁵⁹ 59

Proposition 3. *The firm size distribution behaves, for large S , as the sum of the two Pareto distributions*⁶⁰ 60

$$P(S_i) \sim \frac{C_\alpha}{S_i^{1+\alpha}} + \frac{C_\mu}{S_i^{1+\mu}} \quad (9) \quad 57$$

where $C_\alpha = \left(\frac{\mu}{\mu-1}\right)^{\alpha}$ and $C_\mu = \frac{\alpha}{\mu-1}$ ⁶¹ 62

Proof. See Appendix A.5. □ 33

Since $\alpha < \mu$, this proposition implies that the first term dominates and determines the tail of the size distribution. This case corresponds to a scenario where large firms are most likely made up of a large number of sub-units $K \sim S/\bar{s}$ and the tail of $P(S)$ simply mirrors that of the distribution $P(K)$. The second term, on the other hand, corresponds to much rarer cases where large firms are made up of a handful of large sub-units (hence explaining why the tail behavior has an exponent μ), and are thus poorly diversified. The relative probability that large firms are in this second category, we denote with $\pi(S_i)$, behaves as $(C_\mu/C_\alpha) S_i^{\alpha-\mu}$ and goes to 0 for large S_i . Although it does not provide an explanation to why the number and size of the sub-units should be Pareto distributed,¹² Proposition 3 clarifies that the tail of the firm size distribution inherits its behavior from the distribution featuring the heavier tail between those of the sub-unit size and number.⁶² 62

Conditional distribution of the growth rate volatility. We next move to the distribution of growth rate volatility conditional on size.⁶³ 63

Proposition 4. *The distribution of growth rate volatilities conditional on size S is given, for large S , by*⁶⁴ 64

$$P(\sigma|S) \approx \frac{1 - \pi(S)}{\bar{\sigma}(S)} G\left(\frac{\sigma}{\bar{\sigma}(S)}\right) \left(1 - \frac{\sigma}{\sigma_0}\right)^{\mu-1} + \pi(S) H(\sigma), \quad (10) \quad 64$$

where $\bar{\sigma}(S) \sim S^{-\beta}$ is given by Eq. (7) with $\beta = (\mu - 1)/\mu$, $\pi(S) \sim S^{\alpha-\mu}$ and $H(\cdot)$ is a contribution peaked at $\sigma \approx \sigma_0$. Finally $G(\cdot)$ is defined in Eq. (8) with $G(x) \sim x^{-1-\mu}$.⁶⁴ 64

Proof. See Appendix A.6. □ 48

This proposition states that conditional distribution of the growth rate volatility is a mix of two components weighted with probability $1 - \pi(S_i)$ and $\pi(S_i)$.⁶⁵ 65

The first component reproduces the volatility distribution observed in the previous section under the single granularity hypothesis with the two regimes associated with well and poorly diversified large firms featuring an evenly or skewed distribution of sales among sub-units. This means that the conditional volatility distribution displays a power-law tail regime $\sigma^{-1-\mu}$ with $1 < \mu < 2$ for $\bar{\sigma}(S) \ll \sigma \ll \sigma_0$. Moreover, the growth volatility scales with size as $S^{-\beta}$ with $\beta = (\mu - 1)/\mu$ and not as $S^{-1/2}$ as predicted under the standard Central Limit theorem. Note that all these firms typically have a large number of sub-units.⁶⁶ 66

The second component is new and represents a peculiar feature that emerges when the two granularity sources are combined, something that was overlooked by both Wyart and Bouchaud (2003) and Gabaix (2011). With probability $\pi(S_i)$, large firms can be constituted by a very low number of

¹²There exists a large class of general and intuitive processes that generate Pareto distributions in both K_i and s_{ji} . One example is to assume that the sub-units of a firm grow according to a mixture of stochastic growth and redistribution between them as in $s_{ijt+1} - s_{ijt} = \eta_{ijt+1} s_{ijt} + \gamma \left(\sum_{k=1}^{K_i} s_{ikt} - s_{ijt} \right)$ where the first term accounts for stochastic multiplicative growth and the term with γ for a net flow going from larger sub-units into smaller sub-units. See Bouchaud and Mézard (2000) for details.⁶⁷ 67

sub-units, which mechanically concentrate aggregate sales and prevent diversification. For these firms, the volatility remains of order σ_0 , generating an hump in the distribution around this value. The qualitative behavior of $P(\sigma|S)$ is reported in the right-panel of Figure 2.⁶⁷

Proposition 4 gives the opportunity to clarify the subtle relation between the two set-ups with either one or two sources of granularity. The former can be imagined as fixing the number of sub-units K to $K = S/\bar{s}$, with the consequence of removing the “hump” in the volatility distribution around σ_0 . Indeed, the probability to observe a ill-diversified firm in a single granularity model is of order $S^{-1-\mu}$, which tends to zero much faster than $S^{\alpha-\mu}$, obtained in the case with two sources of granularity.⁶⁸

Using the distribution derived in Proposition 4 we can proceed to study the behavior of its moments.⁶⁹

Proposition 5. For $1 < \alpha < \mu$, the integer moments of the growth rate volatilities conditional to size S are asymptotically given, for large S , by:¹⁹⁸

$$\mathbb{E}[\sigma^q|S] = C_1 S^{1-\mu} + C_2 S^{q\frac{1-\mu}{\mu}} + C_3 S^{\alpha-\mu} + \mathcal{O}\left(S^{\min(\alpha-\mu, 1-\mu, q\frac{1-\mu}{\mu})}\right), \quad (11)$$

where C_1 , C_2 and C_3 are numerical constants.⁷⁰

Proof. See Appendix A.7. ■⁵¹

This proposition states that the dominant behavior of the conditional moments of the volatility is determined by the smallest exponent in the expansion above. When $1 < \alpha < \mu$, all the moments of order greater or equal to 2 ($q \geq 2$) are asymptotically dominated by the third term, $C_3 S^{\alpha-\mu}$, which represents the contribution of large firms with few sub-units. This also happens with the first moment ($q = 1$) if the tail of the distribution of the number of sub-units $P(K)$ is light and satisfies $\alpha > \mu + \frac{1-\mu}{\mu}$.⁷¹ The naive scaling for the first moment, obtained when the second term in Eq. (11) is dominant, only holds when the right tail of $P(K)$ is heavy enough, with $\alpha < \mu + \frac{1-\mu}{\mu}$.⁷² Note finally that the median volatility always scales as $\sigma_{\text{med}}(S) \sim S^{-\beta}$ with $\beta = (\mu - 1)/\mu$. This proposition again confirms that the scaling behavior of volatility moments in this model depends on the moment under consideration.⁷¹

The economics of this proposition can be understood by noticing that firms with large size S can be in this set-up of three different types. The first type is composed by large firms whose sales are evenly distributed among a large number of sub-units. For these firms $S \approx K\bar{s}$ and the HHi is relatively small $\mathcal{H} \approx \mathcal{H}_{\text{typ}}$, meaning they contribute to the moments of the growth volatility by a factor of order $S^{q\frac{1-\mu}{\mu}}$.⁷² The second type is composed by large firms that also have a large number of sub-units. However, the sales of these firms are concentrated in very few sub-units. Again for these firms $S \approx K\bar{s}$, but their HHi is very high and can go up to $\mathcal{H} \approx 1$; their contribution to volatility moments behaves as $S^{1-\mu}$ independently of q . Finally, a fraction of these large firms is made up of only a few sub-units which mechanically results in a very high Herfindahl-Hirschman index ($\mathcal{H} \approx 1$). They therefore will have $\sigma \approx \sigma_0$ and all moments will scale as σ^q independently of S . They contribute to volatility moments by a factor proportional to their relative fraction, $S^{\alpha-\mu}$. This last group was not present in Gabaix (2011) model and was overlooked in Wyart and Bouchaud (2003).⁷²

Distribution of the growth rates. We are now able to provide a complete characterization of the probability distribution of the growth rates. We start with the following proposition.⁷³

Proposition 6. The distribution of growth rates conditional on size S and on growth volatility σ is given, for large S , by:⁷⁰

$$P_S(g|\sigma, S) \approx (1 - \pi(S)) \mathcal{N}(0, \sigma^2) + \pi(S) Q_\eta, \quad (12)$$

where $\mathcal{N}(0, \sigma^2)$ is a Normal distribution with variance $\sigma^2 = \sigma_0^2 \mathcal{H}$ and Q_η a non universal distribution that depends on the distribution of the sub-unit growth shocks η . The weight $\pi(S)$ represents the probability of observing a large firm with only few sub-units vanishing when size grows larger as $S^{\alpha-\mu}$.⁷⁴

Neglecting large firms with a small number of sub-units and integrating Eq. (12) over the first term of the distribution $P(\sigma|S)$ in Eq. (10) gives⁷⁴

$$P(g|S) \sim S^\beta L_{\mu,0}(gS^\beta), \quad \text{when } g \ll 1, \quad (13)$$

where $L_{\mu,0}(\cdot)$ is the symmetric Lévy alpha-stable probability density with stability parameter $1 < \mu < 2$.¹³
 Because of the cut-off in the distribution of σ , this distribution also has a cut-off, with $P(g|S) = 0$ for
 $g \gtrsim S$. The complete distribution $P(g)$ is obtained by integrating over $P(s)$, and behaves asymptotically
 as $P(g) \sim |g|^{-1-\mu}$.⁷⁴

Proof. See Appendix A.8. ■

Before discussing the content of this proposition, recall that a firm's growth rate is defined as the sum of the sub-unit growth shocks weighted by their relative size (cfr. Eq. (2)). Growth volatility is therefore proportional to the square root of the HHi, computed using the sizes of the sub-units (cfr. Eq. (3)). With this in mind, Proposition 6 states that the growth rate distribution, conditional on size and volatility, is again the combination of two components.⁷⁶

The first component is associated with large firms made up by a large number of sub-units, and results from invoking the Central Limit Theorem (CLT henceforth). In the limit of a large number of sub-units, a firm's growth rate g is the sum of a large number of random variables with finite variance; its distribution converges therefore to a Normal distribution. The speed of convergence to this asymptotic limit is not uniform, and depends on the extent to which a firm's size is evenly distributed among its sub-units. However, for a large enough number of sub-units, the Normal distribution provides a good approximation independently of the distribution of the η shocks, as long as it has a finite variance. The second component is instead associated with large firms having only a handful of sub-units, thus preventing the CLT from applying. Their growth rate distribution is therefore strongly determined by that of the sub-unit shocks, η . In the extreme case of a firm with one single sub-unit, the two distributions would coincide.⁷⁷

The second statement in Proposition 6 concerns the behavior of the growth rate distribution when we disregard the role of large firms with few sub-units, and we pool together those with a large number of sub-units but with different growth volatilities (stemming from their very heterogeneous level of diversification). Formally, this exercise consists in mixing together random variables, which are approximately Gaussian, using the conditional volatility distribution $P(\sigma|S)$ as a mixing function.¹⁴ The resulting distribution, $P(g|S) \approx \int d\sigma \mathcal{N}(0, \sigma) P(\sigma|S)$, inherits its behavior from $P(\sigma|S)$ which has a Pareto right tail with exponent $-(1 + \mu)$, and is truncated at σ_0 . Correspondingly, our proposition states that $P(g|S)$ is distributed according to a *truncated* symmetric Lévy alpha-stable distribution with a stability parameter μ . This is consistent with a power law decay with exponent $-(1 + \mu)$, truncated for large growth rates.⁷⁸

Taking stock, we can conclude by discussing the behavior of the unconditional growth rates distribution $P(g)$, which is obtained when we pool together all types of firms. Their heterogeneity in both structure and size is captured by their heterogeneity in growth volatility. This distribution is defined in terms of a Gaussian mixture as $P(g) \approx \int dS d\sigma \mathcal{N}(0, \sigma) P(\sigma|S) P(S)$. Hence, the behavior of the growth rates distribution in this model can be rationalized in terms of a class of statistical models known as Gaussian Mixtures. The basic idea is that mixing together random variables with centered distributions but heterogeneous variances provides a simple and intuitive mechanism to generate continuous, unimodal and heavy-tailed distributions such as the one observed in the data. (Andrews and Mallows, 1974; West, 1987). Such mixtures have also been proposed to explain firm growth rate distributions in Buldyrev et al. (2007).⁷⁹

If this statement holds, then un-mixing the growth rates by rescaling them by the corresponding individual volatility, would lead to an approximately Normal distribution. The quality of this approximation is driven by two factors. First, it's possible that we would observe large firms with few sub-units, whose non-Normal growth rates contaminate the Gaussian mixture. Second, the very heterogeneous sizes of the sub-units which make up a large firm slows down the convergence to the Normal limit induced by the CLT.⁸⁰

¹³Symmetric Lévy alpha-stable distributions are a family of distributions defined with location, scale and stability parameters. This last parameter determines the behavior of the tails of the distribution. When the stability parameter is equal to 2, one obtains a Gaussian distribution, which is a subset of this family. Instead, taking a stability parameter of 1 leads to the Cauchy distribution.⁷⁴

¹⁴This only concerns the first term of $P(\sigma|S)$ in Eq. (10) since we are disregarding large firms with few sub-units.⁷⁸

Aggregation. Before concluding this theoretical section we present a last result describing how the model behaves against aggregation.⁸¹

Proposition 7. *Proposition 3, 4, 5 and 6 are robust against the additive aggregation of firms into (possibly fictitious) supra-firms, or even the whole economic activity of a country.*⁸²

Proof. See Appendix A.9. ■⁸¹

This result has the notable implication the statistical properties we have described above are independent of the level of aggregation of the original sub-units. Merging firms into supra-firms would generate entities whose growth trajectories would be described in a first approximation by Proposition 3, Proposition 4, Proposition 5 and Proposition 6.¹⁵⁸³

3. Empirical investigations⁸⁴

The models analyzed in this paper attempt to explain key statistical regularities in the growth of business firms. Both surmise that these regularities are a consequence of the internal structure of firms. Heterogeneous and granular distributions for the number and sizes of the sub-units of a firm have a direct impact on its growth volatility. In these models, firms can be separated into groups, with well-diversified firms whose size is evenly distributed among several sub-units on the one hand, and firms which are poorly diversified on the other. The second group's poor diversification results either from them being made up of a small number of sub-units, or from a large number of sub-units but whose size is concentrated in only a handful of them. Ultimately, the coexistence of these different firms in a market should determine how their size and growth interact.⁸⁵

These new results translate into more precise testable predictions. Specifically, we focus on three aspects that have received little attention in the literature: the distribution of the growth rate volatilities, its relation with firm size, and finally how it ultimately determines the shape of the growth rate distribution. In performing our investigations one should always keep in mind that our predictions are only sharp in the limit of large firm sizes, $S \rightarrow \infty$. Therefore empirical analysis are expected to show some deviations from these predictions, which should nevertheless taper off as S increases. Before diving in these investigations, we begin by describing our data, empirical proxies and statistical procedures.⁸⁶

3.1. Data, empirical proxies and binning procedure⁸⁷

Our empirical investigations take advantage of the Compustat database collecting financial, statistical and market information on global companies throughout the world. Compustat collects data for medium to large publicly traded companies, and is well known for the quality of its data and for the long time-span it covers. While we are aware of the limitation of the Compustat data in terms of sample selection, we believe that they are high quality data on the US economy with legal entities which are consistently defined in time and breadth, along with high frequency observations which are not typically available in business register data.⁸⁸

From this source, we extract a panel of companies spanning the period from 1961 to 2020 with information collected at the quarterly frequency. For each company, we observe size as proxied by Total Sales,¹⁶ and we deflate nominal sales using the quarterly GDP deflator provided by the Federal Reserve Bank of St. Louis.¹⁷ To limit inconsistencies regarding our size proxy due to different accounting rules, we consider only companies incorporated in the US.⁸⁹

To clarify our data pre-processing, let \tilde{S}_{iqy} represent the size of a firm i in a quarter q and year y expressed in millions of US dollars deflated with a GDP deflator with base year in 2012. We

¹⁵This is an important property of the model since is in line with the available empirical evidence (Lee et al., 1998; Castaldi and Dosi, 2008) and with Gabaix' granularity hypothesis. Moreover while this robustness against aggregation is shared with Gabaix' model, it possesses some discriminatory power: for example, the Sutton (2002) model does not satisfy this property (Wyart and Bouchaud, 2003).¹⁸³

¹⁶The Compustat name for the size proxy is 'sales'.¹⁸⁹

¹⁷We download the 'GDPDEF' quarterly series from the Federal Reserve Economic Data (FRED) web site.⁸⁹

define a normalized quarter size as $S_{iqy} = \frac{N_y \bar{S}_{iqy}}{\sum_{ia} S_{iqy}}$ where N_y represent the number of quarter size observations available in year y . This normalization is important stationarize the size distribution. To simplify the notation, we absorb qy into a time subscript t . Since our data records firm size at the quarterly frequency we define annual growth rates as the logarithmic difference over one year, $g_{it} = \ln(S_{it+4}) - \ln(S_{it})$, rolling over quarters to maximize the number of observations. Similarly when we work with the growth rate of the non-normalized size \bar{S}_{it} . For each firm we then compute a single averaged (across years) normalized size \bar{S}_i , and we investigate its growth dynamics considering the corresponding annual growth rates g_{it} . After removing firms for which we do not observe at least two growth rates, we are left with 24,233 (out of a total of 38,995) companies, corresponding to over one million growth rate observations. Companies in the Compustat sample tend to be large, since they are publicly traded, with an average quarterly Total Sales value of about 450 millions in 2012 USD and a positive average growth rate. For each firm we observe on average 46 growth rates, a number that should limit concerns about the potential noise affecting the firm growth volatility estimates we compute in the paper. Descriptive statistics on the sample used are reported in Appendix B.1.

Finally, to reduce the effect of individual observations when we investigate the relation between a firm's size and its growth dynamics, we implement a pre-processing technique known as data binning. This technique consists in grouping firms based on their size and compute for each group (i.e. bin) some statistics of the corresponding growth rates. In the following, we set the number of bins to 25 and we assign each firm to each bin based on its average normalized size $\bar{S}_i = \frac{1}{T_i} \sum_{t=1}^{T_i} S_{it}$. The bins are defined so that they contain the same number of firms. We then compute for each firm the corresponding growth volatility, proxied by the adjusted mean absolute deviation $\sigma_i = \sqrt{\frac{1}{T_i} \sum_{t=1}^{T_i} |g_{it} - \bar{g}_i|}$, where \bar{g}_i is the sample average growth rate of firm i computed over T_i observations.¹⁸ We then compute the average size and volatility across firms belonging to the same bin. We implement this procedure also for higher absolute moments of the volatility we denote as σ_i^q with $q = 2, 3, 4$.

3.2. Growth rate volatility

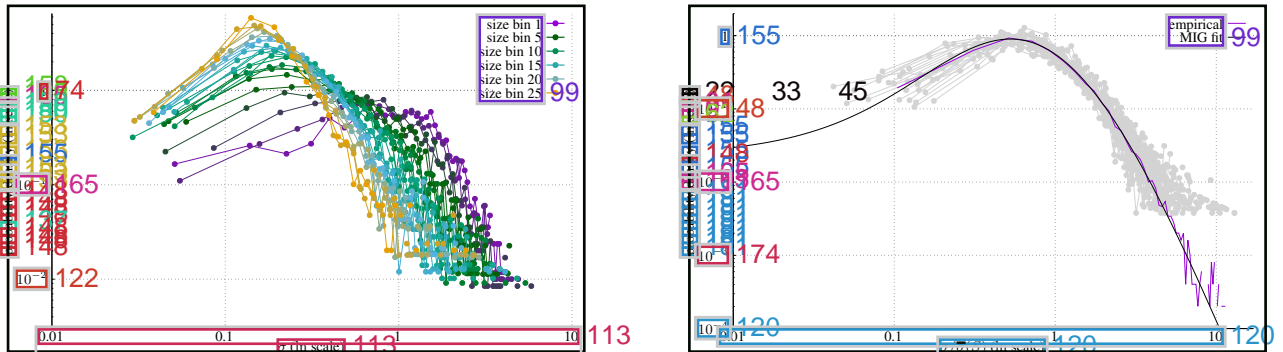
Our first investigation concerns the statistical properties of the growth rate volatility σ_i . Indeed, Proposition 4 describes the distribution of these volatilities conditional on size, allowing to make the following prediction.

Prediction 1. For large size S , the distribution of growth rate volatilities conditioned on size, $P(\sigma|S)$, displays a size-dependent contribution together with a size-independent contribution that appears as a hump at $\sigma = \sigma_0$. Rescaling the volatilities by their average computed over firms of the same size, $\bar{\sigma}(S)$, leads to a curve collapse for the size-dependent contribution into a single master curve displaying a power law tail with exponent $-(1 + \mu)$.

To test this prediction, we start by computing the growth volatility σ_i for each of the 24,233 firms in the sample according to the procedure described in Section 3.1 above. Volatilities range from 0.002 to 5.879 with an average value of 0.479 and a standard deviation of 0.490. We then group volatilities in 25 size bins containing approximately 970 observations each and look at their distributions within the bins. Left-panel of Figure 3 displays the estimated probability density (histogram) for the 25 bins on a double-log scale. Moving from smaller (dark-violet) to larger (gold) firms the distribution shifts smoothly towards the left, pushing the corresponding average volatility from 1.218 to 0.219. The right tail in all the 25 distributions appears to be log-linear, suggesting a power law decay of their densities. We note, however, the absence of a hump for large volatilities representing the size-independent contribution in Prediction 1. Figure 8 in Appendix B.1 reports the distribution of the growth rate volatility on a double log scale for the six size bins 1, 5, 10, 15, 20 and 25. We see no sign of the hump for large volatilities. We confirm our visual inspection with a non-parametric test of bi-modality, which rejects the existence of a second mode at any reasonable level of statistical significance.

¹⁸A bar over a variable indicates from now on the corresponding sample average. In this definition, the correcting factor $\sqrt{\frac{1}{T_i}}$ comes from the observation that for a centered Normal distribution $E[X]/\sqrt{E[X^2]} = \sqrt{\frac{1}{T_i}}$ so that the mean absolute deviation is a low-moment estimator for the standard deviation.

Figure 3: Growth volatility distribution 96



Notes. Left panel reports on a double log scale and for 25 bins, defined in term of normalized size, the distribution of the growth rate volatility. Right panel reports on a double log scale the distribution of the growth volatility rescaled by the average volatility observed in each bin together with a Lognormal (black line) and Inverse Gamma fit (solid line). The ML estimates of the scale, shape and location parameters in the Inverse Gamma fit are found 4.788(0.139), 4.620(0.086) and 0.326(0.010) respectively. In all panels volatility is computed as the mean absolute deviation multiplied by the factor $\sqrt{\pi/2}$. Data source: Compustat. 96

We next construct the rescaled volatilities, $\sigma_i/\bar{\sigma}(S)$, and report the corresponding empirical densities in the right-panel of Figure 3. In line with Prediction 1, all the 25 distributions of the rescaled volatility (light-gray shaded curves) collapse nicely onto a single master curve. We find again no sign of the hump at large volatilities, indicating that $P(\sigma|S)$ is entirely determined by the size dependent contribution in Eq. (10). However, in this case one should consider that the location of the hump in the 25 distributions would move around with the rescaling by $\bar{\sigma}(S)$ because the relative size of the contribution would shift as well, making harder the identification of the humps. 97

Taking stock of this behavior, we investigate the properties of the distribution of the rescaled growth volatility, corresponding to the function G in Eq. (10). We achieve this by pooling together the rescaled volatilities and estimating the resulting density. The histogram we obtain, shown in Figure 3 (dark-violet line), matches the shaded gray area representing the master curve on top of which the 25 binned rescaled histograms collapse. We propose to characterize this empirical histogram with a 3-parameters Modified Inverse Gamma (MIG) density, 98

$$P_{MIG}(x; a, b, m) = C(a, b, m)(x + m)^{-(1+b)} \exp\left(-\frac{a}{x + m}\right), \quad (x \geq 0), \quad (14) \quad 97$$

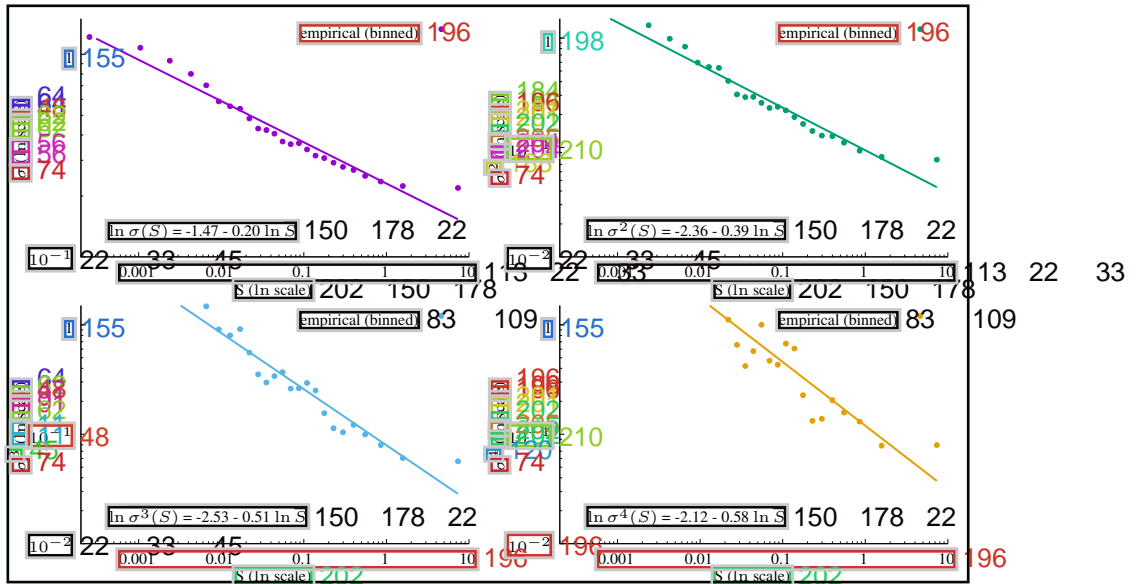
where (a, b, m) represent the scale, shape and location parameter respectively. The normalization constant $C(a, b, m)$ normalizes the distribution when integrating over $\sigma \geq 0$.¹⁹ The reason for this choice is that the Modified Inverse Gamma distribution, as the original Inverse Gamma, features a power law right-tail with exponent equal to $-(1+b)$ for large volatilities. The specific choice of a Modified Inverse Gamma distribution is otherwise purely phenomenological and we do not attribute too much meaning to the small σ behaviour, for which the collapse of the different curves shown in Figure 3 is far from perfect. It is important however that the right tail of the Inverse Gamma is consistent with the power law tail of function G in Eq. (10) resulting, in turn, from the tail of the function F in Eq. (4). 100

A Maximum Likelihood estimation of the parameters yields 4.788(0.139), 4.620(0.086) and 0.326(0.010) for the scale, shape and location parameters respectively. The fit, reported in the right-panel of Figure 3 (solid black-line), describes its empirical target rather well. We conclude that the Modified Inverse Gamma distribution is a good first approximation to describe the function $G(x)$ in Eq. (10). Moreover, this ML fitting procedure provides an indirect estimate of the parameter μ . Since the right-tail of the Modified Inverse Gamma is a power law with exponent $-(1+b)$ and Prediction 1 suggests a power law

¹⁹The normalization constant in the Modified Inverse Gamma density reads $\frac{a^b}{\Gamma(b)}$ while in Eq. (14) we set $C(a, b, m) = \frac{a^b}{\Gamma(b)}$ 100

$\frac{a^b}{\Gamma(b)} \cdot \Gamma(b, \frac{a}{x+m})$ where $\Gamma(b, \frac{a}{x+m})$ is the upper Incomplete gamma function. 100

Figure 4: Size and growth volatility 201



To test this, we bin volatilities according to the same procedure described above. Within each bin, we compute the average normalized size \bar{S}_b and the first 4 moments $\bar{\sigma}^q_b$ with $q = 1, 2, 3, 4$ and plot on a double log scale $\bar{\sigma}^q_b$ against \bar{S}_b . To help the visual inspection of the result, we add the fit of the log-linear relation $\log \bar{\sigma}^q_b = a_0 + a_1 \log \bar{S}_b$. The four panels of Figure 4 display the results.

We begin with the top-left panel of Figure 4, reporting the first moment of the growth volatility σ conditioned on size.²⁰ The decay with size is approximately linear on a double log scale, meaning that volatility decays as a power law. The only major deviation is observed in the bin associated with the largest firms, which tend to have a higher volatility than the one corresponding to the scaling. These firms appear to be less effectively diversified than what the model would lead us to expect.¹⁰⁸

The exponent is found to be about $-0.20(0.01)$, very much in line with the existing literature. When the right tail of the distribution of the number of sub-units $P(K)$ is heavy enough,²¹ this empirical result has an important consequence. Indeed, in this case the estimated exponent has been shown to be $\frac{1-\mu}{\mu}$ ¹⁰⁹ implying $\mu = \frac{1}{1-\alpha} = 1.25$. This estimate is inconsistent with the 4.5 we have found when fitting the distribution of the rescaled growth volatilities.²²¹⁰⁹

This is confirmed by the study of higher order conditional moments. Because $\alpha > 1$, the theory predicts that all of them should decay with size in the same way, as $S^{\alpha-\mu}$. Unfortunately this is not what we observe in the remaining three panels of Figure 2. While they all conform to a power law decay, with possibly the same anomaly that the very largest firms have higher values than expected, they have apparently different scaling exponents, equal to $-0.39(0.02)$, $-0.51(0.03)$ and $-0.58(0.04)$. This is in contradiction with Prediction 2, which states that their scaling should be *independent* of the moment order q and equal to $\alpha - \mu \approx -0.2$. Our evidence suggests in contrast a clear dependence on the order q of the exponent. In fact, the scaling we obtain is close to the one we would observe if the second term in Eq. (11), proportional to $S^{q-\frac{1-\mu}{\mu}}$,¹¹⁰ was the dominant term, which is the result expected for a *thin-tailed* distribution of rescaled volatilities $\sigma/\bar{\sigma}(S)$, i.e. with a tail exponent $b > \mu$, as indeed found above since $b \approx 4.6$. Such a thin-tailed distribution of volatilities would asymptotically lead to exponents -0.4 , -0.6 and -0.8 for $q = 2, 3$ and 4 respectively. We however expect subdominant corrections coming from the incipient tail contribution to be responsible for the observed discrepancies for $q \lesssim b$ (-0.51 instead of -0.6 for $q = 3$ and -0.58 instead of -0.8 for $q = 4$).²³ These results appear again robust when we test them using the standard deviation to proxy growth volatilities and different samples including only firms with at least 20 growth rates and firms closing their fiscal year in December (cfr. Appendix B).¹¹⁰

Summarizing these investigations on growth volatility, we may conclude that although the granularity framework is partially consistent with empirical evidence it also presents major drawbacks. We have indeed shown that the rescaled volatility distribution is independent of size and displays a power-law tail, being overall well approximated by a Modified Inverse Gamma distribution with a thin right tail. However, we do not see any sign of the non-scaling hump the model predicts for large volatilities. Finally, the moments of size-conditioned growth volatility distribution do decay with size as power laws, but with exponents that are not wholly consistent with theoretical predictions.¹¹¹

3.3. Growth rate distribution¹¹²

In this sub-section, our interest moves to the growth rates and their distribution. Considering Proposition 6 is again not trivial, since the use of the asymptotic representations in Eq. (12) and (13) requires to work in the very large size region. In fact, it is only in this region that the Normal approximation associated with the CLT is expected to be valid, and where the Levy alpha-stable regime where $g \sim S^{-\beta}$ is well separated from the non-universal regime where $g \sim 1$ and the growth rate distribution depends on that of the sub-units growth shocks. To make this even more challenging, our results indicate that corrections to the CLT decay slowly, as $S^{1-\mu}$, and that the same is true for

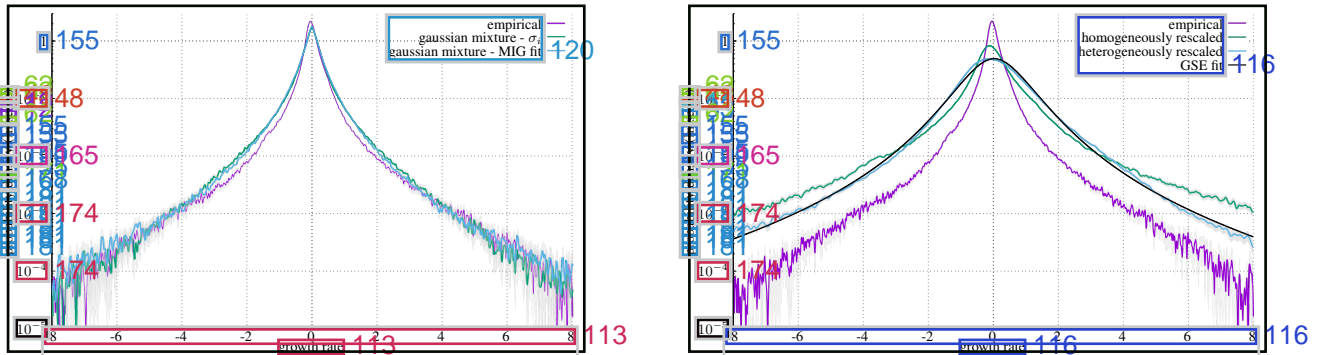
²⁰This is a replica of the right-panel of Figure 1. We report again to clarify how we build it and to facilitate the comparison with the other 3 moments.¹⁰⁸

²¹Heavy enough here means respecting the constraint $\alpha < \mu + \frac{1-\mu}{\mu}$.¹²⁰

²²When the right tail of the distribution $P(K)$ is thin enough, $\alpha > \mu + \frac{1-\mu}{\mu}$, $\mathbb{E}[\sigma|S]$ would scale as $S^{\alpha-\mu}$ implying $\beta = \mu - \alpha = 0.2$.¹²⁰

²³In fact, one predicts an asymptotic behaviour as $S^{-b\beta}$ independent of q whenever $q > b$.¹¹⁰

Figure 5: Growth rate distribution 165



Notes: Left panel reports the kernel estimate of the unconditional empirical density of the annual growth rate of the normalized quarter size after removing its mean and pooling growth rates across firms and year-quarter (purple line). We add the empirical densities estimated using synthetic growth rates obtained by mixing Gaussian random shocks with growth volatilities bootstrapped from those estimated as mean absolute deviation (green line) and sampling from the shifted Inverse Gamma distribution in Eq. (14) (light-blue line). Right panel compares the empirical benchmark (purple line) with the two empirical densities estimated on rescaled annual growth rates obtained by removing their mean and dividing by their volatility. First (green line) we use an homogeneous mean and an homogeneous volatility for the entire sample, second (light-blue line) we use individual specific means and volatilities computed as the leave one out mean absolute deviations. We add a GSE fit for the heterogeneously rescaled growth rates distribution computed on the kernel density estimate (black line). In all plots mean absolute deviations are adjusted by the factor $\sqrt{\pi/2}$. Kernel density estimates are computed with a Gaussian kernel function and a bandwidth chosen according to the normal reference rule-of-thumb. The estimate is evaluated on a 10,000 points regular grid defined over the entire empirical range. We also report the 95% confidence interval. Data source: Compustat. 113

the corrections associated with the existence of large firms with only a handful of sub-units, which vanishes as $S^{\alpha-\beta}$. Unfortunately, typical data-sets contain only a few data points in the large size region, and so we expect finite size corrections to play a significant role in shaping the empirical growth rate distribution. 114

Despite this caveat, Proposition 6 remains effective in offering guidance to look at growth rates and at their distribution allowing us to make a sharp empirical prediction. 115

Prediction 3. *The unconditional growth rate distribution $P(q)$ can be rationalized as a mixture of Normal random variables, that is $P(q)$ is approximately equal to $\int dS d\sigma \mathcal{N}(0, \sigma) P(\sigma|S) P(S)$. Net of finite size corrections, the growth rate distribution conditional on volatility and size, $P(q|\sigma, S)$, is Normal. 116*

To test this prediction, we perform first a numerical exercise where we simulate a growth rate distribution as a scale mixture of Normal random variables. To this aim, we generate 1,000,000 synthetic growth rates as $g_i = \sigma_i \xi_i$ where ξ_i is a Normal random variable with zero mean and unit variance while σ a random variable with a density $P(\sigma)$. The draws from the distribution $P(\sigma)$ are done successively in two different ways. For the first approach, we bootstrap σ from the empirical observations. The second approach assumes an Modified Inverse Gamma density for $P(\sigma)$, with parameters fit using observed volatilities rescaled by their average by size bin as in the right-panel of Figure 3. 117

Our results are reported in the left-panel of Figure 5 (green and light-blue lines respectively). Although some discrepancies are observed, the Gaussian Mixture model generates a growth rate distribution in very good agreement with empirical observation both in the central and tail regions. The two procedures we have implemented produce qualitatively equivalent results, and perform significantly better than the one reported in Figure 1 (green line). The key difference is that in Figure 1, the volatilities used to generate the artificial growth rates were simulated according to $\sigma_i \sim S^{-\beta}$, thus neglecting the heterogeneity associated with a firm's internal structure in terms of number and size of sub-units. The resulting Gaussian mixture produces a distribution that is not able to capture the central cusp and the fat tails of its empirical target. With this respect a further remark is in order. If, in the mixing of the Normal random variables, one uses the MIG fitted on the non-rescaled volatilities the corresponding growth rates display a distribution that, contrary to what happens with rescaled

volatilities, misses its empirical target. Indeed the shape parameter b of the MIG in this case is found to be 2.35(0.03), significantly lower than 4.62(0.09). This implies a fatter right tail for the volatility distribution inducing fatter tails in the distribution of the growth rates generated as scale mixture of Normals. We have clarified above why the estimate of b with non-rescaled volatilities is likely to be biased due to size heterogeneity. This is reassuring when it comes to the sensitivity and consistency of the argument.¹¹⁸

A second exercise, inspired by Prediction 3, concerns the shape of the distribution of growth rates conditional on size and on volatility, which is suggested to be approximately Normal. To test this, we proceed as follows. For each firm in our sample, we compute an average growth \bar{g}_i , and for each of its growth rates g_{it} we compute a growth volatility σ_{it} , computed as the *leave-one-out* mean absolute deviation of the growth rates, obtained from the time-series $g_{it'}$ where the growth rate g_{it} for $t' = t$ has been discarded. We then define the corresponding rescaled growth rates \hat{g}_{it} as $(g_{it} - \bar{g}_i)/\sigma_{it}$. For consistency, we also apply the *leave-one-out* procedure to the mean growth \bar{g}_i .²⁴ The resulting distribution is reported in the right-panel of Figure 5 (light-blue line). It is apparent that the rescaling procedure has a significant effect on the shape of the growth rate distribution, smoothing the central cusp and fattening both tails. These remain clearly non-Gaussian and sub-exponential, since they display a positive convexity in a linear-log representation. In the same figure, we report for comparison the distribution we would obtain by rescaling the growth rates with an homogeneous mean and an homogeneous volatility for the entire sample (green line). This shows that the associated reshaping, although still apparent, is significantly less pronounced. It is equally apparent that the parabolic shape of a Normal distribution would not provide a good fit for the entire distribution.¹¹⁹

We propose a phenomenological model to quantify the extent to which this rescaling procedure move the growth rate distribution towards the predicted Normal benchmark. We therefore consider a parametric family of distributions, that we name Generalized Stretched Exponential (GSE), with density¹²¹

$$P_{GSE}(x; C, u, v, w, z) = C \exp\left(\frac{(x-v)^2}{2u^2(1+(x/w)^{2/z})}\right) \quad (15)$$

where (u, v, w, z) are all positive parameters and C is a normalization constant. This family of distributions is built *ad-hoc* to feature a Gaussian behavior for small x ($x < w$), and a stretched ($z < 1$) or compressed ($z > 1$) exponential decay for large x ($x > w$).²⁵ The case $z = 2$ corresponds to the standard Gaussian, whereas $z \rightarrow 0$ mimics power-law tails. To fit the GSE distribution we proceed as follows. We first compute the kernel density estimate of the central body of the empirical distribution of the heterogeneously rescaled growth rates \hat{g}_i . Next, using a non linear least squares algorithm, we fit the estimated density to recover the GSE parameters.¹²³

Figure 5 reports, in the right-panel, this GSE fit (black line) appearing to a large extent indistinguishable from the empirical distribution, both in the central part and in the tails. This confirms that the proposed family of distributions performs very well in fitting the data. The estimated coefficients are found equal to $C = 0.483(0.004)$, $u = 0.894(0.006)$, $v = -0.006(0.001)$, $w = 1.905(0.020)$ and $z = 0.377(0.003)$. Such a fit allows us to provide a quantitative assessment of the interval over which the distribution can be considered approximately a Gaussian distribution. With an estimated value of w approximately equal to 1.905 the empirical distribution of \hat{g} can be considered Gaussian in the range $[-1.905, 1.905]$. Further, we can compute by numerical integration of the kernel density estimate, that more than 90% of the probability mass falls in this Gaussian regime. As a point of comparison, if one were to consider in the same figure the homogeneously rescaled growth rates (green line) w estimate would reduce to 0.717 and the corresponding probability mass to 70% corresponding to a smaller Gaussian regime.¹²⁴

However, the same GSE fit provides information on the non-Gaussian nature of the two tails.¹²⁶ Indeed the parameter z is found to be significantly smaller than one both for homogeneously and heterogeneously rescaled growth rates identifying stretched exponential tails. Hence tails fatter than those featured by a Gaussian, a fact independently noted also in Larsen-Hallock et al. (2022).²⁶¹²⁶

²⁴The *leave-one-out* procedure avoids an artificial truncation of the tails, see e.g. Bouchaud and Potters (2003).

²⁵More precisely when x is large with respect to w the tails of the density behave proportionally to $\exp[-\frac{x^2}{2w^2}]$.

²⁶In fact Larsen-Hallock et al. (2022) fit the tails with a power-law, which is, over a limited region, not very different

Table 1: Symmetric Generalized Stretched Exponential fit 242 120 22

	C	u	v	w	z	Prob. mass $[-w, w]$	217
<i>Whole sample</i> 217							
homogeneous rescaling	0.764 (0.004)	0.432 (0.002)	0.014 (0.000)	0.673 (0.005)	0.412 (0.001)	0.684	217
heterogeneous rescaling	0.494 (0.003)	0.863 (0.004)	0.023 (0.001)	1.777 (0.015)	0.407 (0.003)	0.897	214
<i>Size bin</i> 216							
1	0.391 (0.006)	1.149 (0.018)	0.067 (0.003)	2.701 (0.084)	0.388 (0.017)	0.949	214
2	0.423 (0.011)	0.982 (0.031)	0.059 (0.004)	1.915 (0.132)	0.603 (0.021)	0.893	214
3	0.428 (0.008)	0.995 (0.020)	0.076 (0.003)	2.084 (0.084)	0.483 (0.015)	0.913	214
4	0.452 (0.010)	0.938 (0.020)	0.048 (0.003)	1.939 (0.077)	0.444 (0.014)	0.903	212
5	0.392 (0.006)	1.227 (0.013)	-0.009 (0.003)	3.468 (0.060)	0 (0.018)	0.979	212
6	0.51 (0.010)	0.786 (0.017)	0.023 (0.002)	1.43 (0.055)	0.51 (0.010)	0.835	212
7	0.474 (0.006)	0.941 (0.009)	0.002 (0.002)	2.123 (0.036)	0.301 (0.008)	0.927	212
8	0.458 (0.007)	1.008 (0.011)	-0.004 (0.002)	2.445 (0.046)	0.231 (0.011)	0.95	212
9	0.488 (0.007)	0.908 (0.011)	-0.023 (0.002)	2.013 (0.044)	0.323 (0.009)	0.923	212
10	0.471 (0.007)	0.969 (0.012)	0.003 (0.002)	2.291 (0.049)	0.265 (0.011)	0.942	212
11	0.483 (0.009)	0.899 (0.014)	-0.019 (0.002)	1.919 (0.055)	0.397 (0.011)	0.912	212
12	0.462 (0.007)	0.99 (0.013)	-0.018 (0.002)	2.35 (0.054)	0.322 (0.011)	0.948	212
13	0.449 (0.007)	1.01 (0.013)	-0.034 (0.002)	2.413 (0.055)	0.282 (0.012)	0.947	212
14	0.499 (0.012)	0.839 (0.020)	-0.013 (0.003)	1.65 (0.072)	0.475 (0.013)	0.88	212
15	0.472 (0.010)	0.946 (0.017)	-0.021 (0.003)	2.147 (0.070)	0.336 (0.015)	0.934	212
16	0.468 (0.007)	0.987 (0.011)	0.015 (0.002)	2.396 (0.045)	0.241 (0.010)	0.95	212
17	0.489 (0.010)	0.883 (0.016)	0.003 (0.002)	1.844 (0.063)	0.43 (0.012)	0.906	212
18	0.457 (0.011)	0.988 (0.019)	-0.016 (0.003)	2.326 (0.079)	0.308 (0.017)	0.945	212
19	0.5 (0.012)	0.846 (0.019)	-0.017 (0.003)	1.717 (0.069)	0.427 (0.013)	0.894	212
20	0.508 (0.011)	0.823 (0.017)	0.029 (0.002)	1.633 (0.058)	0.434 (0.011)	0.882	212
21	0.48 (0.007)	0.919 (0.012)	0.055 (0.002)	2.051 (0.046)	0.327 (0.010)	0.925	212
22	0.536 (0.013)	0.713 (0.019)	0.028 (0.003)	1.204 (0.059)	0.546 (0.010)	0.799	212
23	0.518 (0.010)	0.782 (0.016)	0.024 (0.002)	1.476 (0.052)	0.462 (0.010)	0.859	212
24	0.541 (0.013)	0.672 (0.019)	0.052 (0.002)	1.073 (0.053)	0.563 (0.009)	0.77	212
25	0.516 (0.012)	0.742 (0.018)	0.084 (0.003)	1.335 (0.055)	0.474 (0.010)	0.84	212
<i>Time window</i> 174							
2 years	0.449 (0.003)	1.046 (0.006)	0.008 (0.001)	2.643 (0.029)	0.303 (0.006)	0.966	171
3 years	0.442 (0.004)	1.121 (0.006)	0.004 (0.001)	3.196 (0.031)	0.185 (0.007)	0.985	171
4 years	0.44 (0.004)	1.173 (0.005)	0.001 (0.001)	3.668 (0.028)	0.011 (0.008)	0.993	171

Notes: estimates are obtained with a non linear least square algorithm applied to kernel density estimates evaluated on a regular grid in the interval $[-8, 8]$. This procedure is applied to homogeneously rescaled growth rates, and heterogeneously rescaled growth rates in different size bins and computed over different time windows. Data source: Compustat.

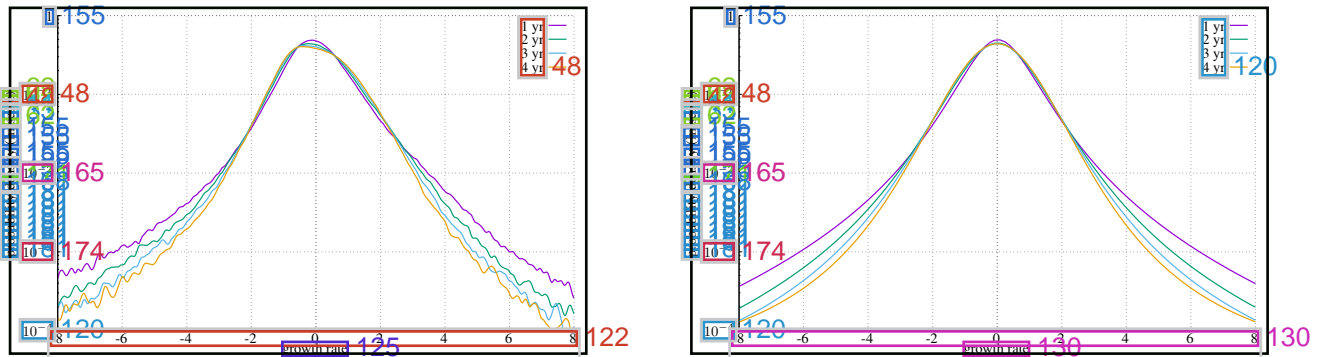
126

Taking stock of these findings, it looks fair to say that our data provide a mixed and contrasting evidence in support to Proposition 6. On one side the Gaussian Mixture model seems to work properly, at least in a first approximation, as an explanation for the existence of a central cusp and of fat tails in the empirical growth rate distribution. In line with the proposition un-mixing the growth rates by rescaling them by the corresponding individual mean and volatility, lead to an important extension of the Gaussian regime in their empirical distribution. However the tails are not absorbed within the Gaussian regime and remain fatter, significantly departing from the strict Gaussian Mixture model. Whether this is due to a flaw in the model rather than to significant finite size corrections is what we attempt to investigate with the last two exercises performed in the remaining of this section. 127

As discussed in the theory section the quality of the Gaussian approximation for the un-mixed growth rates is driven by two factors. First, it is possible that we would observe large firms with few sub-units, whose non Gaussian growth rates contaminate the Gaussian mixture. Second, the very heterogeneous sizes of the sub-units which make up a large firm slows down the convergence to the Normal limit induced by the CLT. Driven by these considerations we perform two investigations. 128

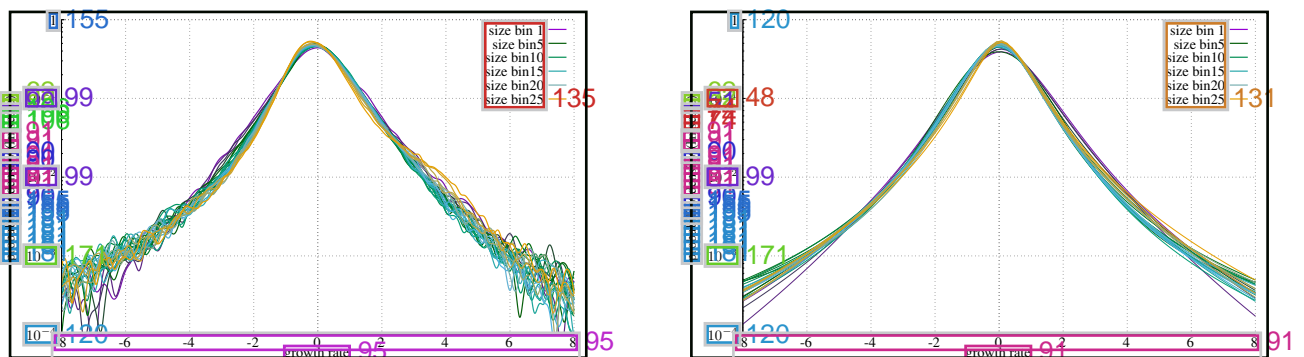
First, we exploit the fact that in a model where the growth rate g_i , computed over a one year time window, is a random variable with a GSE distribution multiplied by a firm specific volatility, then the corresponding growth rates, computed over a larger time span, is obtained as the sum of the random variables g_i . If these growth rates are independent and identically distributed, the Central Limit Theorem mechanism comes into play, which should lead to a progressive “Gaussianization” of the

from a stretched exponential with the observed low value of z . 126



Notes: Left panel Kernel density estimates are computed with a Gaussian kernel function and a bandwidth chosen according to the normal reference rule-of-thumb. The estimate is evaluated on a 2,500 points regular grid defined over the interval $[-8, 8]$. Right panel Symmetric GSE fits computed with a non linear least square algorithm applied to density estimates. Tim-window over which growth rates are computed increases from 1 to 4 years moving from dark-violet, to green, blue and gold colors. Data source: Compustat.

Figure 7: Rescaled growth rate distribution (size bins) 130



Notes: Left panel Kernel density estimates are computed with a Gaussian kernel function and a bandwidth chosen according to the normal reference rule-of-thumb. The estimate is evaluated on a 2,500 points regular grid defined over the interval $[-8, 8]$. Right panel Symmetric GSE fits computed with a non linear least square algorithm applied to density estimates. Bin size increases moving from dark-violet, to green, blue and gold colors. Data source: Compustat.

distribution of the corresponding un-mixed growth rates \hat{g}_i . Figure 6 shows that this is what happens empirically albeit with some intriguing discrepancies. It reports in the left panel the kernel density estimate of the distributions of the rescaled growth rate computed over a 1, 2, 3 and 4 years time-span together with, in the right panel, their GSE fit whose parameters estimates are shown in the bottom panel of Table 1. In line with our reasoning, we observe an apparent process of “Gaussianization” of the distribution. The size of the Gaussian central region, measured by w , almost double rising from 1.9 to 3.5 when we widen the time window from 1 year to 4 years. Perhaps surprisingly, however, the tails (described by the parameter z) appear to get *fatter* as the time-span increases (see Table 1), although the probability mass in that region significantly drops from 9% at 1 year to less than 1% at 4 years. Correspondingly, when comparing the empirical distribution for 2 years, 3 years and 4 years to a numerical convolution of 2, 3 or 4 i.i.d. random variables drawn from the 1 year distribution, we find significant deviations: the tails of empirical distributions are “too fat”, signalling the existence of persistence effects. In other words, the convolution results suggests that growth rates are autocorrelated even over three and four years, i.e. persistently good or bad periods or persistently volatile periods build up tails that would not exist if the growth process was independent across time.

In a second, final exercise we investigate the size dependency of the rescaled growth rates distribution. To this aim we bin firms in 25 groups according to their average size \bar{S}_i following the same procedure described in the data section and used to investigate the growth volatility distribution in Section 3.2. Figure 7 reports in the left panel the kernel density estimate of the distributions for the 25 bins

together with, in the right panel, their GSE fit whose parameters estimates are shown in the middle panel of Table 1. Visually all distributions fall approximately on one another, suggesting that, once un-mixed using idiosyncratic means and volatilities, the distribution of growth rate looks universal and independent of size. [131]

In other words we see *no sign* of “Gaussianization” for larger sizes, contrarily to what we were expecting. Such visual inspection is confirmed by the parameters estimates reported in Table 1 where we do not observe any clear trend in any of the key parameters. If anything the parameter w defining the Gaussian region actually *decreases* with firm average size \bar{S} , together with the probability mass in the interval $[-w, w]$ which drops from approximately 0.95% for small firms to 0.84 for the largest firms. [132]

This observation means that rescaled growth rates of small firms are *more Gaussian* than those of large firms, which goes against the intuition provided by Prediction 3. This result may be related to the fact that the exponent β is smaller for large firms, indicating that – somewhat paradoxically – the activity of large firms is more volatile than one might have anticipated from the $S^{-\beta}$ scaling. Similarly z does not show a clear trend with size, remaining for all bins well below the threshold identifying stretched exponential tails and showing a rather good deal of homogeneity across bins and with respect to the results obtained pooling together all firms. [133]

4. Conclusions [134]

This paper shows that granular models of firm growth, as those in Wyart and Bouchaud (2003) and Gabaix (2011), do not provide a convincing explanation of the empirically robust scaling of the growth volatility with firm size, $\sigma \sim S^{-\beta}$, with an exponent β lower than 0.5. Nor do they account, as a consequence, for the shape of the distribution of the growth rates of business firms. [135]

The basic “granular” assumption rationalizes such anomalous scaling by the concentration of the sales of firms across sub-units which would be dominated by only few of them representing for example blockbuster products or large customers, as in Herskovic et al. (2020). Although enticing, such a picture leads to falsifiable predictions, in particular concerning the distribution of volatility conditional to size, for which we provided new theoretical results. Quite remarkably, and as predicted by theory, this distribution is indeed close to universal (i.e., independent of firm size) once rescaled by the average size dependent volatility $S^{-\beta}$. However, the tail of this universal distribution is much too “thin” to be compatible with the granularity hypothesis. [136]

Similarly, we do *not* observe the anomalous scaling of higher moments of the growth rate volatility with firm size that should reflect the presence of a cohort of very poorly diversified firms. The data unambiguously rejects this prediction. At the same time, and again contrary to what is predicted by models, after accounting for idiosyncratic volatilities growth rate shocks remain non-Gaussian and fat tailed. Correspondingly, high moments of growth rates but *not* of their volatility are dominated by such tail events, a result also noted in Larsen-Hallock et al. (2022). [137]

These findings reveal more unanswered questions. Where do such very large idiosyncratic shocks come from? Why are large firms even *more* volatile than expected, and with more weight in the non-Gaussian tails? While this paper shows that the answers to these questions cannot be searched for in granular mechanisms alone it is not aimed at proposing alternative explanations. One intriguing possibility is that shocks hitting a firm’s sub-units become more and more correlated as its size increases, due either to supply chain effects affecting inputs or customers common to all sub-units, or to reputation shocks that impact the whole firm. Although such an analysis goes beyond the scope of the present paper, we have explored this hypothesis finding encouraging evidence: both the correlation of a firm’s growth rate with that of the whole economy and the correlation of the growth rate of firms of similar sizes clearly *grow* with their size. Very much along the lines of Herskovic et al. (2020), we surmise that this feature is the key missing ingredient to fully account for the observed statistics of firm growth. [138]

Acknowledgments 139

We want to thank E. Larsen-Hallock, A. Rej and D. Thesmar for sharing their results with us and 140
for discussions. JM wishes to thank M. Benzaquen, D. Farmer, A. Fosset, F. Lafond, L. Mungo, M. 140
Tomas and M. Riccaboni for numerous discussions on the topic of firm growth modeling. We also 140
thank participants at the 2023 Computations in Economics and Finance conference (Nice) for helpful 140
comments. 140

References 237

- AMARAL, L. A. N., S. V. BULDYREV, S. HAVLIN, H. LESCHHORN, P. MAASS, M. A. SALINGER, H. E. STANLEY, AND M. H. STANLEY (1997): "Scaling Behavior in Economics: I. Empirical Results for Company Growth," *Journal de Physique I*, 7, 621–633. 235
- AMEIJEIRAS-ALONSO, J., R. CRUJEIRAS, AND A. RODRÍGUEZ-CASAL (2019): "Mode testing, critical bandwidth and excess mass," *Test*, 28, 900–919. 244
- ANDREWS, D. F. AND C. L. MALLOWS (1974): "Scale Mixtures of Normal Distributions," *Journal of the Royal Statistical Society. Series B (Methodological)*, 36, 99–102. 245
- AXTELL, R. L. (2001): "Zipf Distribution of U.S. Firm Sizes," *Science*, 293, 1818–1820. 246
- BOUCHAUD, J.-P. AND M. MÉZARD (2000): "Wealth condensation in a simple model of economy," *Physica A: Statistical Mechanics and its Applications*, 282, 536–545. 247
- BOUCHAUD, J.-P. AND M. POTTERS (2003): *Theory of financial risks (2nd Edition)*, vol. 12, Cambridge University Press, Cambridge From Statistical Physics to Risk. 248
- BULDYREV, S. V., F. PAMMOLLI, M. RICCABONI, AND H. E. STANLEY (2020): *The rise and fall of business firms: A stochastic framework on innovation, creative destruction and growth*, Cambridge University Press. 249
- BULDYREV, S. V., M. RICCABONI, J. GROWIEC, H. E. STANLEY, AND F. PAMMOLLI (2007): "The Growth of Business Firms: Facts and Theory," *Journal of the European Economic Association*, 5, 574–584. 250
- CASTALDI, C. AND G. DOSI (2008): "The patterns of output growth of firms and countries: Scale invariances and scale specificities," *Empirical Economics*, 37, 475–495. 251
- DERRIDA, B. (1997): "From Random Walks to Spin Glasses," *Physica D: Nonlinear Phenomena*, 107, 186–198. 252
- DOSI, G. (2023): *The Foundations of Complex Evolving Economies: Part One: Innovation, Organization, and Industrial Dynamics*. The Foundations of Complex Evolving Economies, Oxford University Press. 253
- FONTANELLI, L., M. NAPOLETANO, AND A. SECCHI (2024): "Uncovering the inverse J-Shaped Relationship between Firm Growth Rate Volatility and Size." Unpublished. 254
- FU, D., F. PAMMOLLI, S. V. BULDYREV, M. RICCABONI, K. MATIA, K. YAMASAKI, AND H. E. STANLEY (2005): "The growth of business firms: Theoretical framework and empirical evidence," *Proceedings of the National Academy of Sciences*, 102, 18801–18806. 255
- GABAIX, X. (2009): "Power Laws in Economics and Finance," *Annual Review of Economics*, 1, 255–294. 256
- (2011): "The Granular Origins of Aggregate Fluctuations," *Econometrica*, 79, 733–772. 257
- GIBRAT, R. (1931): *Les inégalités économiques: applications: aux inégalités des richesses, à la concentration des entreprises, aux populations des villes, aux statistiques des familles, etc., d'une loi nouvelle, la loi de l'effect proportionnel*. Recueil Sirev. 258
- GNEDENKO, B. V. AND A. N. KOLMOGOROV (1953): *Distributions for Sums of Independent Random Variables*, Addison-Wesley Publishing Co. 259
- HALTIWANGER, J. (1997): "Measuring and analyzing aggregate fluctuations: the importance of building from microeconomic evidence," *IMF Review*, 55–78. 260
- HERSKOVIC, B., B. KELLY, H. LUSTIG, AND S. VAN NIEUWERBURGH (2020): "Firm volatility in granular networks," *Journal of Political Economy*, 128, 4097–4162. 261
- HYMER, S. AND P. PASHIGIAN (1962): "Firm Size and Rate of Growth," *Journal of Political Economy*, 70, 556–569. 262
- KRAMARZ, F., J. MARTIN, AND I. MEJEAN (2020): "Volatility in the small and in the large: The lack of diversification in international trade," *Journal of International Economics*, 122, 103276. 263
- LARSEN-HALLOCK, E., A. REJ, AND D. THESMAR (2022): "Expectations Formation with Fat-tailed Processes: Evidence from Sales Forecasts." ArXiv 2210.10169. 264
- LEE, Y., L. A. N. AMARAL, D. CANNING, M. MEYER, AND H. E. STANLEY (1998): "Universal features in the growth dynamics of complex organizations," *Physical Review Letters*, 81, 3275–3278, arXiv: cond-mat/9804100. 265
- MORAN, J. AND M. RICCABONI (2024): "Compositional Growth Models," ArXiv 2404.07935. 266
- SCHWARZKOPF, Y., R. L. AXTELL, AND J. D. FARMER (2010): "The cause of universality in growth fluctuations," ArXiv 1004.5397. 267
- STANLEY, M. H. R., L. A. N. AMARAL, S. V. BULDYREV, S. HAVLIN, H. LESCHHORN, P. MAASS, M. A. SALINGER, AND H. E. STANLEY (1996): "Scaling behaviour in the growth of companies," *Nature*, 379, 804–806. 268
- SUTTON, J. (1997): "Gibrat's Legacy," *Journal of Economic Literature*, 35, 40–59. 269
- (2002): "The variance of firm growth rates: the 'scaling' puzzle," *Physica A: Statistical Mechanics and its Applications*, 312, 577–590. 270
- WEST, M. (1987): "On scale mixtures of normal distributions," *Biometrika*, 74, 646–648. 271
- WYART, M. AND J.-P. BOUCHAUD (2003): "Statistical models for company growth," *Physica A: Statistical Mechanics and its Applications*, 326, 241–255. 272

A. Analytical results and proofs 142

Single granularity hypothesis [Gabaix' model] 25

A.1. Preliminary results 120

We begin by considering a single firm consisting of a deterministic number of sub-units K of sizes (s_1, \dots, s_K) distributed according to Assumption 2. With the aim of studying the statistics of the firm's Herfindahl-Hirschman index \mathcal{H} of the sub-unit size we will first establish the scaling of the typical (modal) value of \mathcal{H} by estimating the numerator and the denominator of \mathcal{H} , before computing its moments explicitly and deriving its whole distribution. Without loss of generality, we will take $s_0 = 1$. Indeed, under the current hypotheses it is easy to see that $\mathbb{E}[s] = \frac{1}{K} \sum s_i$ and so taking $s_0 = 1$ amounts to redefining the units in which sub-unit sizes are counted. 145

The following lemmas establish three preliminary results. 146

Lemma 1. The typical value of the Herfindahl index scales with K as 147

$$\mathcal{H}_{typ} \sim K^{2-\frac{1-\mu}{\mu}} 148 K \gg 1. \quad (16) \quad 147$$

Proof. Starting from the definition $\mathcal{H} = \sum_j (s_{ji}/\sum_k s_{ki})^2$, note that by the law of large numbers since $\mathbb{E}[s] < \infty$ we have that $\sum_j s_j \approx K\mathbb{E}[s]$. On the other hand, the expectation of the numerator $\sum_i s_i^2$ is divergent, since $\mathbb{E}[s^2] = \infty$. 148

However, the largest element s_{max} of (s_1, \dots, s_K) scales as $s_{max} \sim K^{\frac{1}{\mu}}$, since it solves 148

$$\int_{s_{max}}^{\infty} ds P(s) \approx \frac{1}{K^{\frac{1}{\mu}}} \frac{1}{158} \quad (17) \quad 148$$

leading to $s_{max}^{-\mu} \approx K^{-1}$. The sum $\sum_i s_i^2$ can be approximated by $s_{max}^2 \approx K^{\frac{2}{\mu}}$, which diverges superlinearly as $K \rightarrow \infty$. 148
Pooling these results together, we obtain 148

$$\mathcal{H}_{typ} \sim \frac{K^{\frac{2}{\mu}}}{K^2 \mathbb{E}[s]^2} 152 K^{2-\frac{1-\mu}{\mu}}. \quad (18) \quad 150$$

□ 165

Lemma 2. The moment generating function of sub-unit sizes $g(\lambda) = \mathbb{E}[e^{-\lambda s}]$ has an expansion 165

$$g(\lambda) \approx 1 - \lambda \mathbb{E}[s] - \lambda^\mu \mu \Gamma[-\mu] + \mathcal{O}(\lambda^\mu). \quad (19) \quad 149$$

which corresponds to the Laplace transform of a probability density decaying as $s^{-1-\mu}$. 149

Proof. This extends results obtained by Derrida (1997). By direct computation 79 7 16

$$\begin{aligned} g(\lambda) &= \frac{1}{70} \frac{\int_0^\infty 22 \cdot 33 \cdot 45}{ds} \frac{d\mathbb{P}(s)}{158} (-\lambda s) = \frac{1}{181} \frac{\int_0^\infty 174}{ds} \frac{d\mathbb{P}(s)}{178} (-\lambda s) \quad 174 \\ &\stackrel{\text{setting } s_0 = 1 \text{ and changing variable } \lambda s = t}{=} \mu \lambda^\mu \int_0^\infty dt \frac{t^{\mu-1}}{174} \exp(-t) \quad 171 \\ &\stackrel{\text{J. 149}}{=} \mu \lambda^\mu \Gamma(-\mu, \lambda) = \mu \lambda^\mu [\Gamma[-\mu] - \gamma(-\mu, \lambda)] \quad 165 \\ &\quad [\Gamma(\cdot, \cdot) \text{ and } \gamma(\cdot, \cdot) \text{ are the upper and lower incomplete gamma functions}] \quad 242 \quad 120 \quad 22 \\ &= -\lambda^\mu \Gamma[-\mu + 1] - \mu \lambda^\mu \sum_{k=0}^{\infty} \frac{(-\lambda)^k}{k!} \frac{\Gamma(\mu+k+1)}{\Gamma(\mu+1)} \quad 148 \\ &= -\lambda^\mu \Gamma[-\mu + 1] + 1 - \lambda \sum_{k=0}^{\infty} \frac{\mu^k}{\mu-1} \frac{\Gamma(\mu+k+1)}{\Gamma(\mu+1)} \quad 150 \quad 158 \\ &= 1 - \lambda^\mu \Gamma[-\mu + 1] - \lambda \mathbb{E}[s] + \mathcal{O}(\lambda^\mu). \quad (20) \quad 165 \end{aligned}$$

□ 165

A useful corollary follows. 151

Corollary 1. The expansion for $\mathbb{E}[s^k e^{-\lambda s}]$ reads 152

$$\mathbb{E}[s^k e^{-\lambda s}] \approx \frac{\mu}{\mu-k} 165 \mu \Gamma[k-\mu] \lambda^{\mu-k} + \frac{\mu \lambda}{1-\mu} 165 + \mathcal{O}(\lambda^{\min(1, \mu-k)}). \quad (21) \quad 165$$

Proof. Note that

$$\begin{aligned} & \frac{d^k g(\lambda)}{d\lambda^k} \Big|_{\lambda=0} = \mathbb{E} \left[\frac{\lambda^k}{1 - \lambda e^{-\lambda s}} \right] = \mathbb{E} \left[(-s)^k e^{-\lambda s} \right] \\ & \quad \text{for } k=0, 1, 2, \dots \end{aligned}$$

so that $\mathbb{E}[s^k e^{-\lambda s}] = (-1)^k g^{(k)}(\lambda)$. Differentiating the expression in the second to last line of Eq. (20) yields the result. \blacksquare 154

Lemma 3. The integer moments of the Herfindahl read

$$\mathbb{E} [\mathcal{H}^k] \approx K^{1-\mu} \mathbb{E}[s]^{-\mu} \mu \frac{\Gamma[\mu]}{\Gamma[2k]} \frac{\Gamma[2k-\mu]}{\Gamma[2k]} 169(K^{1-\mu}) \quad (23)$$

for $k > 1$. In particular, the average Herfindahl scales as $\mathbb{E}[\mathcal{H}] \sim N^{1-\mu}$. 154

Proof. We use the following representation: 155

$$\frac{1}{x^k} = \frac{1}{\Gamma(k)} \int_0^\infty \lambda^{k-1} e^{-\lambda x} d\lambda. \quad (24) \quad 120$$

Indeed, changing variables first as $t = \lambda x$ gives $\int_0^\infty dt t^{k-1} e^{-\lambda x t} = e^{-\lambda x} \int_0^\infty dt t^{k-1} e^{-t} = e^{-\lambda x} \Gamma[k]$. Now write $\mathcal{H}^k = \left(\sum_{i_1} \dots \sum_{i_k} s_{i_1}^2 \dots s_{i_k}^2 \right)^{2k}$ so that using the identity in Eq. (24) we have that

We will now work out the case $k = 1$ before generalising for $k > 1$. Eq. (25) becomes

$$\begin{aligned}
& \mathbb{E}[\mathcal{H}] = \mathbb{E} \left[\int_0^\infty d\lambda \lambda e^{-\lambda} \sum s_i^2 \right] \stackrel{(165)}{=} 165 \\
& \stackrel{(148)}{=} \mathbb{E} \left[\int_0^\infty d\lambda \lambda e^{-\lambda} \sum s_i^2 \right] + \sum_{i>1} 155 \stackrel{(165)}{=} 165 \\
& \stackrel{(155)}{=} \mathbb{E} \left[\int_0^\infty d\lambda \lambda e^{-\lambda} \sum s_i^2 \right] + \sum_{i>1} 155 \stackrel{(165)}{=} 165 \\
& \stackrel{(155)}{=} \mathbb{E} \left[\int_0^\infty d\lambda \lambda e^{-\lambda} \sum s_i^2 \right] + \sum_{i>1} 155 \stackrel{(171)}{=} 171 \\
& \stackrel{(181)}{=} \mathbb{E} \left[\int_0^\infty d\lambda \lambda e^{-\lambda} \sum s_i^2 \right] + \sum_{i>1} 155 \stackrel{(171)}{=} 171 \\
& \stackrel{(180)}{=} K \int_0^\infty d\lambda \lambda \mathbb{E}[s_1^2 e^{-\lambda s_1}] \mathbb{E}[e^{-\lambda s}]^{K-1} \stackrel{(183)}{=} 183
\end{aligned}$$

(26) 155

We now use the results of Lemma 2 and Corollary 1, so that to leading order 177

$$\mathbb{E} [e^{-\lambda s}]^{N-1} \approx (1 - \lambda \mathbb{E}[s])^{K-1} \approx e^{-\lambda \mathbb{E}[s]K}, \quad (27)$$

and 155

$$\mathbb{E}[s^2 e^{-\lambda s}] \approx \mu \Gamma[2 - \mu] \lambda^{\mu - 2}. \quad (28) \quad 168$$

Plugging into the integral, we obtain **155**

$$\begin{aligned} \mathbb{E}[\mathcal{H}] &\approx \mu\Gamma[2-\mu]K \int_0^\infty \frac{22}{22} \frac{33}{33} \frac{45}{45} ds \exp(-45-\lambda K\mathbb{E}[s]) \lambda^{\mu-2} \quad 171 \\ &\quad \boxed{\text{d}\lambda \quad 180} \\ &\approx \mu\Gamma[2-\mu]K \int_0^\infty \frac{180}{180} d\lambda \lambda^{\mu-1} \exp(-\lambda K\mathbb{E}[s]) \quad 171 \\ &\quad \boxed{\text{d}\lambda \quad 180} \\ &\quad \boxed{\text{changing variables } t = \lambda K\mathbb{E}[s] \quad 174} \quad (29) \quad 155 \\ &\approx \mu\Gamma[2-\mu]K^{1-\mu}\mathbb{E}[s]^{-\mu} \int_0^\infty dt t^{\mu-1} e^{-\lambda t} \quad 171 \\ &\quad \boxed{\text{d}t \quad 180} \\ &\approx K^{1-\mu}\mu\Gamma[2-\mu]\Gamma[\mu]\mathbb{E}[s]^{-\mu}, \quad 174 \end{aligned}$$

so that $\mathbb{E}[\mathcal{H}] \sim K^{1-\mu}$. In the general case, we may proceed in similar fashion. 16 7 26

$$= K \mathbb{E} [s^{2k} e^{-\lambda s}] \mathbb{E} [e^{-\lambda s}]^{K-1} + k(K-1) \mathbb{E} [s^{2k+2} e^{-\lambda s}] \mathbb{E} [s^2 e^{-\lambda s}] \mathbb{E} [e^{-\lambda s}]^{K-2} + \dots$$

so that we may split the different contributions as 155

$$\mathbb{E}[\mathcal{H}^k] = \frac{1}{\Gamma(2k)} \int_0^\infty \lambda^{2k-1} \left(K \mathbb{E}[s^{2k} e^{-\lambda s}] \mathbb{E}[e^{-\lambda s}]^{K-1} + k(K-1) \mathbb{E}[s^{2k-2} e^{-\lambda s}] \mathbb{E}[s^2 e^{-\lambda s}] \mathbb{E}[e^{-\lambda s}]^{K-2} + \dots \right) d\lambda$$

= $I_1 + I_2 + \dots$, 155

where I_ℓ is the integral with $j_1 = j_2 = \dots = j_\ell = 1$ in the sum of Eq. (30). We next have to leading order in λ

$$\mathbb{E}[s^{2k} e^{-\lambda s}] \mathbb{E}[e^{-\lambda s}]^{K-1} \approx \mu \Gamma[2k - \mu] e^{-\lambda \mathbb{E}[s] K} \lambda^{\mu - 2k}, \quad (32)$$

so that 153

$$I_1 \approx \frac{K\mu\Gamma[2k-\mu]}{\Gamma[2k]} \int_{\frac{1}{42} \cdot \frac{17}{180}}^{\infty} \frac{\lambda^{33}}{\lambda^{22}} \cdot \frac{\lambda^{45}}{\lambda^{22}} \cdot \lambda^{\mathbb{E}[s]K} \approx \mu K^{1-\mu} \mathbb{E}[s]^{-\mu} \frac{\Gamma[2k]}{\Gamma[2k]} \cdot 22 \cdot 33 \cdot 45 \quad (33)$$

with subleading corrections that are $\mathcal{O}(K^{1-\mu})$. Regarding I_2 , we have that 173

$$\mathbb{E}[s^{2k-2}e^{-\lambda s}] \mathbb{E}[s^2e^{-\lambda s}] \mathbb{E}[e^{-\lambda s}]^{K-2} \approx \mu^2 \Gamma[2k-2-\mu] \Gamma[2-\mu] e^{-\lambda \mathbb{E}[s]} K \lambda^{\mu-2k-2} \lambda^{\mu-2} \propto \lambda^{2\mu-2k}, \quad (34)$$

so that $I_2 \sim K^{1-2\mu} = \mathcal{O}(K^{1-\mu})$. In the end, the dominating contribution is given by I_1 for $k \geq 1$, and so finally **155**

$$\mathbb{E}[\mathcal{H}^k] = K^{1-\mu} \mu \mathbb{E}[s]^{-\mu} \frac{\Gamma[2k] - \mu \Gamma[\mu]}{\Gamma[2k]} \text{169} \left(K^{1-\mu} \right). \quad (35)$$

165

A.2. Proof of Proposition 1.

Proposition 1. For fixed $K \gg 1$, the distribution of the Herfindahl-Hirschman index takes the following form. 68 79 5

$$P(\mathcal{H}|K) = K^{2(\mu-1)/\mu} F(\mathcal{H} K^{2(\mu-1)/\mu}) (1 - \sqrt{\mathcal{H}})^{\mu-1}, \quad (36)$$

with $F(x) \sim \frac{1}{x^{1/\mu}} / 157$ when $1 \ll x \lesssim K^{2(\mu-1)/\mu}$. 165

Proof. Following what we obtained previously, we recognise the Beta function $B(a, b) = \frac{\Gamma(a)\Gamma(b)}{\Gamma(a+b)}$ in Eq. (23) and write 158

$$\begin{aligned} \frac{\Gamma[2k]}{\Gamma[2k-\mu-1]} &= \frac{1}{\Gamma[\mu+1]} \int_0^1 dx x^{2k-\mu-1} (1-x)^{\mu-1} \quad 165 \\ &\stackrel{h=x}{=} \int_0^1 dh h^{k-1-\frac{\mu}{2}} (\sqrt{h})^{\mu-1} \quad 171 \\ &\stackrel{h=180}{=} \int_0^{180} dh h^{k-1-\frac{\mu}{2}} (\sqrt{h})^{\mu-1} \quad 171 \end{aligned}$$

However, because we can identify $\mathbb{E} [\mathcal{H}^k] = \int_0^1 d\mathcal{H} P(\mathcal{H})\mathcal{H}^k$, it follows that we can identify the leading contribution to this integral, coming from the region $\mathcal{H} \approx 1$. 158

$$P(\mathcal{H}) \sim \mathcal{H}^{-1 - \frac{\mu}{2}} \left(\frac{155}{\pi} \sqrt{\mathcal{H}} \right)^{\mu-1}. \quad (38)$$

Supplementing this with the fact that the typical value of \mathcal{H} should be $\mathcal{H}_{\text{typ}} \sim K^{2-\frac{1}{\mu}}$, this supposes that for $\mathcal{H} \ll 1$ we should have a scaling form. 158

$$P(\mathcal{H}) \approx \frac{1}{\text{Pr}_{\text{hyp}}} \left(\frac{\mathcal{H}}{\mathcal{H}_{\text{hyp}}} \right)^{\frac{165}{2}} \quad (39) \quad 165$$

that is such that $F(x) \sim x^{-1-\mu/2}$ for large $x \sim \frac{1}{\mathcal{N}_{\text{typ}}}$ in consistency with the form given in Eq. (37). Furthermore, this is consistent with the fact that for large K , the typical Herfindahl reads 158

$$\mathcal{H} \approx \text{[red box]}_1 \text{[green box]}_2 \text{[blue box]}_3 s_i, 165$$

and so the generalised law of large numbers indicates that $\sum_i s_i^2$ will have a distribution that is a Lévy-stable distribution with parameter $\mu/2$. The factor $(1 - \sqrt{\mathcal{H}})^{1-\mu}$ reconciles this with the fact that the Herfindahl is bounded by 1 and with the fact that entities with $\mathcal{H} \approx 1$ are statistically unlikely. Finally note that writing $\sigma \propto \sqrt{\mathcal{H}}$ leads to Eq. (8). ■

A.3. Proof of Proposition 2. 165

Proposition 2. For all $q > 0$, the moments of \mathcal{H} conditional on K are given, to the leading order, by 82 79 68

$$\mathbb{E}[\mathcal{H}^q|K] \approx C_1 K^{1-\mu} + C_2 K^{2q} \frac{1-\mu}{\mu} \frac{\sqrt{22} \min(133_{\mu, 2q}, 145_{\mu})}{160} \frac{1}{739} \frac{1}{783} \frac{1}{74} \frac{1}{7} - 153^{33} 155^{45} \quad (41) \quad 74$$

where C_1 and C_2 are two constants.

Proof. We write the generalised moment as 161

$$\mathbb{E}[\mathcal{H}^q] = \int_0^{f^1_{\text{typ}}} \frac{d\mathcal{H}}{\mathcal{H}_{\text{typ}}} \left(\frac{165}{165 - \mathcal{H}_{\text{typ}}} \right)^{\mu-1} 165$$

$$= \mathcal{H}_{\text{typ}}^q \int_0^{f^1_{\text{typ}}} dx \frac{165}{165 - x\mathcal{H}_{\text{typ}}} \left(1 - \sqrt{x\mathcal{H}_{\text{typ}}} \right)^{\mu-1} \frac{99}{165} 18$$

We may then approximate this integral using the intermediate tail of F , noting also that F introduces a lower cut-off to the integral. The integral therefore runs from $\mathcal{H} \approx \mathcal{H}_{\text{typ}}$ to $\mathcal{H} \approx 1$. Therefore, 180

$$\mathbb{E}[\mathcal{H}^q] \sim \mathcal{H}^d \quad \boxed{\int_{\frac{1}{2}}^{1/\mathcal{H}_{\text{typ}}} 202 \frac{22}{dx} \frac{33}{q-\mu/2} \frac{33}{(1-\sqrt{x}\mathcal{H}_{\text{typ}})^2} \frac{\mu-1}{2} \frac{22}{33} \frac{33}{45} \frac{45}{45}} \quad (43) \quad 83$$

Next, we introduce $u = \sqrt{x\mathcal{H}_{\text{typ}}}$, with $dx = 2\frac{u}{\mathcal{H}_{\text{typ}}} du$ and the integral runs from $u = \sqrt{\mathcal{H}_{\text{typ}}}$ to $u = 1$. Therefore,

$$\begin{aligned} \mathbb{E}[\mathcal{H}^q] &\sim 2\mathcal{H}_{\text{typ}}^{q/2} \frac{\Gamma(1+\mu/2)}{\Gamma(2q-\mu+1)} u^{2q-\mu-1} (1-u)^{\mu-1} \quad 99 \\ &\sim 2\mathcal{H}_{\text{typ}}^{q/2} \left[\frac{f_1}{48} u^{2q-\mu-1} (1-u)^{\mu-1} - \frac{f_2}{48} u^{2q-\mu-1} (1-u)^{\mu-1} \right] \quad 99 \\ &\sim 2\mathcal{H}_{\text{typ}}^{q/2} B_{\frac{2q-\mu}{2}, \mu} - 2\mathcal{H}_{\text{typ}}^{q/2} B_{\frac{2q-\mu}{2}, \mu} \quad 165 \end{aligned}$$

where $B(a, b)$ is the Beta function described above, and $B_x(a, b) = \int_0^x dt t^{a-1} (1-t)^{b-1}$ is the incomplete Beta function. 165
 Using then that $B_x(a, b) = \frac{x^a}{\Gamma(a)} B(a, b)$ (161 $\mathcal{O}(x)$), we have finally that 165

$$\mathbb{E}[\mathcal{H}^q] \sim B(2q - \mu, \mu) \mathcal{H}_{\text{typ}}^{\mu/2} \frac{1}{2q - \mu + 1} \frac{\partial \mathcal{H}^q}{\partial p} \Big|_{p=0} \quad (45)$$

which, after plugging in $\mathcal{H}_{typ} \sim K^{2/\mu}$, yields the result given above. In addition to this, it becomes clear from the computation that the contribution $\mathcal{H}_{typ}^{1/\mu}$ comes from the values close to $\mathcal{H} \approx \mathcal{H}_{typ}$, while the contribution $\mathcal{H}_{typ}^{1/\mu}$ comes from the tail.

Double granularity hypothesis [Wyart and Bouchaud's model] 55

A.4. Preliminary results 99

²⁷ The statistical object of interest in this set-up is $P(S, R)$,²⁷ the joint distribution describing firms of size S that experience an absolute size change R between t and $t + 1$. Formally, we may write this as

$$P(S, R) = \sum_{K \geq 1} p(K) \left[\int_0^\infty \prod_{i=1}^K ds_i p(s_i) \delta \left(S - \sum_{j=1}^K s_j \right) \int_0^\infty \prod_{i=1}^K d\eta_i p(\eta_i) \delta \left(R - \sum_{j=1}^K \eta_j s_j \right) \right] 22 \quad 33 \quad 45$$

(46) 202

where $\delta(\cdot)$ is a Dirac delta distribution. Equation (46) represents $P(S, R)$ as the sum over all possible arrangements of Gaussian shocks, sub-unit numbers and sub-unit sizes that result in an initial size equal to S and to an absolute growth equal to R . The role of the Dirac delta is to impose the constraints $S = \sum_i s_j$ and $R = \sum_j \eta_j s_j$, and gives this representation the structure of a sum of convolutions over the different variables of interest. 166

Next, we ground the study of this object on three pillars. We first exploit the convolutional structure of Equation (46) by taking the Fourier-Laplace transform with respect to S and R respectively, defining thus

$$\widehat{P}(\lambda, q) := \mathbb{E} [e^{iqR - \lambda S}] = \frac{\int_0^\infty e^{iqR - \lambda S} ds}{\int_0^\infty ds} \exp(iqR - \lambda S) P(S, R) . \quad (47)$$

Indeed, the function $\bar{P}(\lambda, q)$ may be used to retrieve several properties of the distribution $P(S, R)$. For example, when $q = 0$, $\bar{P}(\lambda, q = 0)$ becomes the Laplace transform of the marginal distribution $P(S)$. This can be used to study the behavior of the firm size distribution in the large S limit, which is determined by the behavior of $\bar{P}(\lambda, q = 0)$ in the limit $\lambda \rightarrow 0$.¹⁶⁸

Secondly, Equation (47) implies that

$$-\frac{\partial^2 \widehat{P}(\lambda, q)}{\partial q^2} \Big|_{q=0} = \int_0^\infty \frac{22}{dS} \frac{33}{P(S) \exp(-\lambda S)} \frac{45}{f(\overline{D}R, \overline{D}S)} \Big|_{(164)} . \quad (48)$$

Thus, computing the second derivative of the Fourier-Laplace transform of $P(S, R)$ at $q = 0$ yields the conditional variance of the absolute growth R , which will be relevant when studying the variance of growth rates R/S conditional on firm sizes S .¹⁷²

²⁷To ease the notation, we drop the firm index i and the time index t . 164

Thirdly and finally, once $P(S)$ is characterized, plugging $P(S, R) = P(S)P(R|S)$ into (47) leads to 242 120 214

$$\hat{P}(\lambda, q) = \int_{\frac{7}{16}}^{\infty} dS \int_{\frac{7}{16}}^{\infty} dR \exp(iqR - \lambda S) P(S) P(R|S) , \quad (49)$$

which can be used to identify the distribution of firm growth rates conditional on size. Because the properties of the marginal $P(S)$ can be understood using the technique described above, one is left with the problem of solving for a marginal distribution $P(R|S)$ to match the right-hand side of the equation with the left hand side given by the Fourier-Laplace transform. 175

The following lemmas establish two preliminary results providing a convenient representation of $\bar{P}(\lambda, q)$ and some insights on its behavior. 176

Lemma 4. The Fourier-Laplace transform $\hat{P}(\lambda, q)$ can be represented as

$$\widehat{P}(\lambda, q) = \sum_{K=1}^{\infty} p(K) [1 - g(\lambda, q)]^K, \quad (50)$$

$$\text{where } g(\lambda, q) = \frac{1}{168} (s_1 [1 - 36(-q^2 s^2/2 - \lambda s)]). \quad 174$$

Proof. Plugging (46) into (47) gives

$$\begin{aligned} \hat{P}(\lambda, q) &= \frac{\int_{-\infty}^{\infty} ds}{180} \int_{-\infty}^{20} dr \exp(iqR - \lambda S) \sum_{K \geq 1} p(K) \int_{-\infty}^{\infty} ds_j \int_{-\infty}^{16} d\eta_j p(s_j) \delta(r - s_j) \prod_{i=1}^{29} \int_{-\infty}^{\infty} ds_i \int_{-\infty}^{17} d\eta_i p(\eta_i) \delta(r - \eta_i) \\ &= \sum_{K \geq 1} \frac{1(35)}{185} \int_{-\infty}^{\infty} ds_j \int_{-\infty}^{17} d\eta_j p(s_j) \delta(r - s_j) \prod_{i=1}^{29} \int_{-\infty}^{\infty} ds_i \int_{-\infty}^{17} d\eta_i p(\eta_i) \delta(r - \eta_i) \exp(-\lambda S) \int_{-\infty}^{\infty} dr \int_{-\infty}^{\infty} d\eta_i p(\eta_i) \exp(iqR) \\ &= \sum_{K \geq 1} \frac{1(35)}{185} \int_{-\infty}^{\infty} ds_j \int_{-\infty}^{17} d\eta_j p(s_j) \delta(r - s_j) \prod_{i=1}^{29} \int_{-\infty}^{\infty} ds_i \int_{-\infty}^{120} d\eta_i p(\eta_i) \delta(r - \eta_i) \exp(-\lambda S) \int_{-\infty}^{\infty} dr \int_{-\infty}^{\infty} d\eta_i p(\eta_i) \exp(iqR) \end{aligned}$$

33 4

33 3

22 175

22 174

22 171

22 170

22 169

22 168

22 167

22 166

22 165

22 164

22 163

22 162

22 161

22 160

22 159

22 158

22 157

22 156

22 155

22 154

22 153

22 152

22 151

22 150

22 149

22 148

22 147

22 146

22 145

22 144

22 143

22 142

22 141

22 140

22 139

22 138

22 137

22 136

22 135

22 134

22 133

22 132

22 131

22 130

22 129

22 128

22 127

22 126

22 125

22 124

22 123

22 122

22 121

22 120

22 119

22 118

22 117

22 116

22 115

22 114

22 113

22 112

22 111

22 110

22 109

22 108

22 107

22 106

22 105

22 104

22 103

22 102

22 101

22 100

22 99

22 98

22 97

22 96

22 95

22 94

22 93

22 92

22 91

22 90

22 89

22 88

22 87

22 86

22 85

22 84

22 83

22 82

22 81

22 80

22 79

22 78

22 77

22 76

22 75

22 74

22 73

22 72

22 71

22 70

22 69

22 68

22 67

22 66

22 65

22 64

22 63

22 62

22 61

22 60

22 59

22 58

22 57

22 56

22 55

22 54

22 53

22 52

22 51

22 50

22 49

22 48

22 47

22 46

22 45

22 44

22 43

22 42

22 41

22 40

22 39

22 38

22 37

22 36

22 35

22 34

22 33

22 32

22 31

22 30

22 29

22 28

22 27

22 26

22 25

22 24

22 23

22 22

22 21

22 20

22 19

22 18

22 17

22 16

22 15

22 14

22 13

22 12

22 11

22 10

22 9

22 8

22 7

22 6

22 5

22 4

22 3

22 2

22 1

22 0

[since integrands are independent] 178

$$= \sum_{K>1} \left[\frac{p(\beta\eta)}{178} \int_0^\infty ds \int_0^1 d\eta \, p(s)p(\eta) \exp(iq\eta s - \lambda s) \right]^{99}_{174} \stackrel{174}{=} 33$$

[integrating over η] 178

$$= \sum_{K>1} \left[\frac{f(s)}{p(s)} \right] ds p(s) \exp\left(-\frac{q^2 s^2}{2}\right)$$

$$= \sum_{K>1} p(178) [1 - q(\lambda, q)]^K . \quad 181$$

174

Lemma 4 generates two useful corollaries characterizing the behaviour of $q(\lambda, q)$ for $q = 0$ and in the limit where $\lambda, q \rightarrow 0$ with the product $q\lambda^{-1/\mu}$ constant. The first exploits the assumption that both the number and the size of sub-units are Pareto-distributed, with exponents α and μ respectively and with $1 < \alpha < \mu < 2$. 179

Corollary 2. The Fourier-Laplace transform $\hat{P}(\lambda, q)$ at $q = 0$ reads 174

$$\hat{P}(\lambda, 0) = 1 - \lambda \mathbb{E}[s] \mathbb{E}[K] - \lambda^\alpha \mathbb{E}[s]^\alpha \Gamma[-\alpha + 1] - \lambda^\mu \mathbb{E}[K] \Gamma[-\mu + 1] + \mathcal{O}\left(\lambda^{\max(\alpha, \mu)}\right), \quad (51)$$

where $\mathbb{E}[s]$ and $\mathbb{E}[K]$ are the expected values of the sub-unit size and of the number of sub-units and $\Gamma[\cdot]$ is the gamma function. 100

Proof. We start by computing the Laplace transform of the distribution of the sub-unit size $P(s) = \frac{u}{s+u}$ from Lemma 2 and Eq. (20), we have directly that 174

$$g(\lambda, 0) = \frac{f_1^\infty}{91} \frac{22}{1458s} \frac{33}{150} \frac{45}{(-\lambda s)} = 1 - \lambda^\mu \Gamma[-\mu + 1] - \lambda \mathbb{E}[s] + \mathcal{O}(\lambda^\mu). \quad (52)$$

More generally, the Laplace transform of a power-law distribution with a tail $P(s) \sim s^{-1-\mu}$ with $1 < \mu < 1$, has the form $1 - A\lambda - B\lambda^\mu + \mathcal{O}(\lambda^\mu)$ with A and B two constants that depend on μ . Thus we can obtain the Laplace transform of the distribution of the number of sub-units, $p(K)$, by changing the roles $\alpha \leftrightarrow \mu$. 181

Now, setting $q = 0$ in Equation (50) one gets 174

$$\begin{aligned} \widehat{P}(\lambda, 0) &\approx \sum_{K \geq 1} p(K) [1 - g(\lambda, 0)]^K \quad 181 \\ &\approx \sum_{K \geq 1} p(K) [1 - \lambda^\mu \Gamma[-\mu + 1] - \lambda \mathbb{E}[s]]^K \quad 128 \\ &\quad \text{approximating } (1 - x)^K \text{ with } \exp(-Kx) \quad 51 \\ &\approx \sum_{K \geq 1} p(K) \exp(-K\lambda^\mu \Gamma[-\mu + 1] - K\lambda \mathbb{E}[s]) \quad 99 \\ &\quad \text{setting } v = \lambda^\mu \Gamma[-\mu + 1] + \lambda \mathbb{E}[s] \quad 174 \\ &\approx \int_0^\infty ds P(K) \exp(-vK) \quad 45 \\ &\quad \text{using Equation (52) and Assumption 2} \quad 33 \\ &\approx 1 - v^\alpha \Gamma[-\alpha + 1] - v \mathbb{E}[K] \quad 33 \\ &\approx 1 - (\lambda^\mu \Gamma[-\mu + 1] + \lambda \mathbb{E}[s])^\alpha \Gamma[-\alpha + 1] - (\lambda^\mu \Gamma[-\mu + 1] + \lambda \mathbb{E}[s]) \mathbb{E}[K] \quad 33 \\ &\quad \text{since, by Assumption 3, } 1 < \alpha < \mu < 2 \quad 51 \\ &\approx 1 - \lambda^\alpha \mathbb{E}[s]^\alpha \Gamma[-\alpha + 1] - \lambda^\mu \mathbb{E}[K] \Gamma[-\mu + 1] - \lambda \mathbb{E}[s] \mathbb{E}[K] + \mathcal{O}(\lambda^\alpha) \quad 48 \end{aligned}$$

□ 174

Note that this result intuitively implies that $\mathbb{E}[S] = \mathbb{E}[s]\mathbb{E}[K]$, which means that the average size of a firm is given by the product of the average number of subunits in a firm by the average size of a subunit. This can be obtained directly by noting that $\mathbb{E}[S] = \frac{\partial \widehat{P}(\lambda, 0)}{\partial \lambda}$. 182, 174

The second corollary describes the behaviour of $P(\lambda, q)$ in the limit where $\lambda, q \rightarrow 0$, but keeping $q\lambda^{-1/\mu}$ constant. 183
This corollary will later allow us to compute the distribution $P(R|S)$ in the scaling region where R is proportional to $S^{\frac{1}{\mu}}$. 183

Corollary 3. The Fourier-Laplace transform $\widehat{P}(\lambda, q)$ computed in the limit $\lambda, q \rightarrow 0$ where $q\lambda^{-1/\mu} = \theta$ reads 242 120 214

$$\widehat{P}(\lambda, q = \theta\lambda^{1/\mu}) = 1 - \lambda \mathbb{E}[K] (\mathbb{E}[s] + \mu s_0^{\frac{1}{\mu}} I(\mu)) \mathcal{O}(\lambda), \quad (53) \quad 22 \quad 33$$

where $I(\mu) = \int_0^\infty dt e^{-(1+\mu)t} (1 - e^{-t^2/2}) = -2^{-(1+\mu)/2} \Gamma(-\frac{\mu}{2})$. 134

Proof. As for the previous lemma we start by computing 185

$$\begin{aligned} q(\lambda, q = \theta\lambda^{1/\mu}) &= \int_0^\infty ds P(s) \left(1 - \exp \left(\frac{\theta^2 \lambda^{\frac{2}{\mu}} s^2}{2} \right) \right)^{165} \quad 165 \\ &\quad \text{using the linear approximation of } -e^{-x} \quad 174 \\ &\equiv \int_0^\infty ds P(s) \left(1 - \exp \left(\frac{\theta^2 \lambda^{\frac{2}{\mu}} s^2}{2} \right) \right)^{168} \left(\frac{1}{2} \lambda s \right)^{150} \mathcal{O}(\lambda) \quad 155 \\ &= \lambda \mathbb{E}[s] + \int_0^\infty ds \frac{\mu s^{\frac{1}{\mu}}}{s^{1-\frac{1}{\mu}}} \left(1 - \exp \left(\frac{\theta^2 \lambda^{\frac{2}{\mu}} s^2}{2} \right) \right)^{165} \left(\frac{1}{2} \lambda s \right)^{155} \mathcal{O}(\lambda) \quad 155 \\ &= \lambda \left[\mathbb{E}[s] + \int_0^\infty dt \frac{1}{t^{\frac{1}{\mu}}} \left(1 - e^{-\frac{\theta^2 \lambda^{\frac{2}{\mu}} t^2}{2}} \right)^{171} \right] \mathcal{O}(\lambda) \quad 155 \\ &= \lambda (\mathbb{E}[s] + \mu (s_0 \theta)^\mu I(\mu)) + \mathcal{O}(\lambda). \quad (54) \quad 173 \end{aligned}$$

Plugging (54) in Equation (50) one gets 174

$$\widehat{P}(\lambda, q = \theta\lambda^{1/\mu}) = \sum_{K \geq 1} p(K) [1 - \lambda (\mathbb{E}[s] + \mu (s_0 \theta)^\mu I(\mu)) + \mathcal{O}(\lambda)]^K \quad 171$$

approximating $(1 - x)^K$ with $1 - Kx$ and evaluating the sum with its integral representation 214
 $= 1 - \lambda \mathbb{E}[K] (\mathbb{E}[s] + \mu (s_0 \theta)^\mu I(\mu)) + \mathcal{O}(\lambda)$. 212 (55) 188

□ 174

Finally, the second Lemma states that the second derivative of the Fourier-Laplace transform $\frac{\partial^2 \widehat{P}(\lambda, q)}{\partial q^2}$, evaluated at 171
 $q = 0$, is proportional to $\lambda^{\mu-2}$. More generally, $\frac{\partial^2 \widehat{P}(\lambda, q)}{\partial q^2}$ 188 $\lambda^{\mu-2\ell}$ at $q = 0$ and as $\lambda \rightarrow 0$. 186

Lemma 5. When $1 < \mu < 2$, $-\frac{\partial^2 \hat{P}(\lambda, q)}{\partial q^2}$ evaluated at $q = 0$ behaves as $\lambda^{\mu-2}$, that is 120

$$\frac{\partial^2 \hat{P}(\lambda, q)}{\partial q^2} \Big|_{q=0} \sim \lambda^{\mu-2} \cdot 62$$

(56) 155

Proof. Plug Equation (50) in $-\frac{\partial^2 \hat{P}(\lambda, q)}{\partial q^2}$ obtain 171

$$\begin{aligned} -\frac{\partial^2 \hat{P}(\lambda, q)}{\partial q^2} \Big|_{q=0} &= 2 \frac{\partial}{\partial(q^2)} p(K) [1 - g(\lambda, q)]^K \Big|_{q=0}^{158} \\ &= 2 \frac{\partial}{\partial(q^2)} p(K) \exp(-g(\lambda, q)K) \Big|_{q=0}^{167} \\ &= 2 \frac{\partial g(\lambda, q)}{\partial(q^2)} \Big|_{q=0}^{178} K p(K) \exp(-K g(\lambda, 0)) \Big|_{q=0}^{168} \end{aligned}$$

Computing the derivative at $q = 0$ gives 188

$$2 \frac{\partial g(\lambda, q)}{\partial(q^2)} \Big|_{q=0}^{155} \approx \int_0^\infty ds s^2 e^{-\lambda s} \approx \int_0^\infty ds s^{\mu-1} 120 e^{-\lambda s} \approx s_0^\mu \frac{\Gamma(2-\mu)}{120-\mu} \Big|_{q=0}^{174}$$

Thus we find, for $\lambda \rightarrow 0$ 188

$$\begin{aligned} -\frac{\partial^2 \hat{P}(\lambda, q)}{\partial q^2} \Big|_{q=0}^{258} &\sim 1^\mu \frac{\Gamma(2-\mu)}{120-\mu} \frac{120}{120} K p(K) \exp(-K g(\lambda, 0)) \Big|_{q=0}^{155} \\ &\sim s_0^\mu \frac{\Gamma(2-\mu)}{120-\mu} \frac{120}{120} K p(K) e^{-K} \sim \lambda^{\mu-2} \Big|_{q=0}^{168} \end{aligned}$$

where we've approximated $e^{-K g(\lambda, 0)} \approx e^{-K}$ and used that $\sum_{K>1} K p(K) e^{-K}$ is a finite constant. ■ 188

A.5. Proof of Proposition 3. 192

Proposition 3. The firm size distribution behaves, for large S , as the sum of the two Pareto distributions 190

$$P(S_i) \sim \frac{C_\alpha}{S_i^{\alpha+1}} + \frac{C_\mu}{S_i^{\mu+1}} \quad (57) \quad 155$$

where $C_\alpha = (\frac{\mu}{\alpha-1})^{\frac{\alpha}{\alpha-1}}$ and $C_\mu = (\frac{\alpha}{\mu-1})^{\frac{\alpha}{\mu-1}}$ 174

Proof. This is a direct consequence of Corollary 2. Since $\hat{P}(\lambda, 0)$ is the Laplace transform of the firm size distribution $P(S)$, for sufficiently large S its behavior is described by Equation (51). Gathering the terms proportional to $\lambda^\alpha \Gamma[-\alpha + 1]$ and $\lambda^\mu \Gamma[-\mu + 1]$ allows us to find the asymptotic behaviour described above and the relative contributions of each component by identifying the Laplace transforms of power-law tails. Since the inverse of the Laplace transform of a probability distribution is unique, Proposition 3 follows. Noting that the last line implies that the firm size distribution is asymptotically proportional to 191

$$P(s) \sim \mathbb{E}[s]^\alpha S^{-1-\alpha} + \mathbb{E}[K] S^{-1-\mu}, \quad (58) \quad 188$$

by getting the terms proportional to $\lambda^\alpha \Gamma[-\alpha + 1]$ and $\lambda^\mu \Gamma[-\mu + 1]$ in the expansion above, we may also write this as 191

$$P(s) \sim S^{-1-\alpha} (1 + CS^{\alpha-\mu}), \quad (59) \quad 191$$

where C is a constant. 191

■ 196

A.6. Proof of Proposition 4. 189

Proposition 4. The distribution of growth rate volatilities conditional on size S is given, for large S , by:

$$P(\sigma|S) \approx \frac{1}{G(S)} \frac{\pi(S)}{G(S)} \frac{(\sigma/\bar{\sigma})^{22}}{(11/\bar{\sigma})^{22}} \frac{(\sigma/\mu)^{-1}}{(\pi(S)H(\sigma))^{45}} \quad 68 \quad 82(60) \quad 78$$

where $G(\cdot)$ is defined in Eq. (8), $\bar{\sigma} \sim S^{-\beta}$ is given by Eq. (7) with $\beta = (\mu - 1)/\mu$, $\pi(S) \sim S^{\alpha-\mu}$ and finally $H(\cdot)$ is a contribution peaked at $\sigma \approx \sigma_0$. In particular, $G(x) \sim x^{-1-\mu}$. 193

Proof. Following Proposition 3, firms of size S are made up of two distinct fractions: those for which $S \approx K\mathbb{E}[s]$, which corresponds to the $S^{-1-\alpha}$ tail of the distribution with the exponent α indicating that firms in that tail are large because they have a large number of sub-units, and those firms for which $K = \mathcal{O}(1)$ but are still large because one single sub-unit is large, i.e. $S \approx s_{\max}$, thereby contributing with a tail with weight $S^{-1-\mu}$. The latter firms have $\mathcal{H} \approx 1$.¹⁹⁴

Because of the relative contributions of the tails, the fraction of poorly diversified firms is $\pi(S) \sim S^{\alpha-\mu}$, as highlighted above. We may therefore write that¹⁹⁴

$$P(\sigma|S) = (1 - \pi(S))P(\sigma|S, \text{many subunits}) + \pi(S)P(\sigma|S, \text{few subunits}). \quad (61)$$

◻ 196

Because poorly diversified firms have K of order 1 and are concentrated in a single sub-unit, their Herfindahl is of order 1 and so $P(\sigma|S, \text{poorly diversified}) = H(\sigma)$ is a distribution peaked at σ_0 for all S . Regarding the contribution of firms with $S \propto K$, their Herfindahl is distributed as described in Eq. (8). It follows that¹⁹⁵

$$P(\sigma|S, \text{well diversified}) = \frac{1}{\sqrt{2\pi}} \frac{\sigma}{\sqrt{S}} e^{-\frac{\sigma^2}{2S}} \left(1 - \frac{\sigma}{\sqrt{S}} \right)^{\mu-1}, \quad (62)$$

where $F(\cdot)$ is the function defined in Eq. (4). Since $F(x) \sim x^{-1-\mu/2}$ it follows that $G(x) \sim x^{-1-\mu}$ for large x .⁸ Proposition (4) follows.⁸

A.7. Proof of Proposition 5.¹²⁰

Proposition 5. For $1 < \alpha < \mu$, the integer moments of the growth rate volatilities conditional to size S are asymptotically given, for large S , by:¹⁹³

$$\mathbb{E}[\sigma^q|S] = C_1 S^{1-\mu} + C_2 S^{q-\frac{1-\mu}{\mu}} + \mathcal{O}(S^{\min(\alpha-\mu, 1-\mu, q-\frac{1-\mu}{\mu})}) \quad (63)$$

where C_1 , C_1 and C_3 are numerical constants.²⁸ 198

Proof. As before, we may write this as¹⁹⁷

$$\mathbb{E}[\sigma^q|S] = (1 - \pi(s)) \int_0^\infty \sigma^q dP(\sigma|S, \text{many subunits}) + \pi(S) \int_0^\infty \sigma^q P(\sigma|S, \text{few subunits}), \quad (64)$$

and where the second contribution corresponds to firms with $\mathcal{H} \approx 1$. The second contribution will therefore always give¹⁹⁹

$$\pi(S) \int_0^\infty \sigma^q d\sigma \approx \pi(S) \sim S^{\alpha-\mu}. \quad (65)$$

The case of firms with many subunits is slightly different. Noting that $\sigma \propto \mathcal{H}^{1/2}$, we use the result given in Proposition 1, substitute $q \rightarrow q/2$ and use $K \propto S$ to obtain¹⁹⁹

$$(1 - \pi(s)) \int_0^\infty \sigma^q dP(\sigma|S, \text{many subunits}) \approx \int_0^\infty \sigma^q P(\sigma|S, \text{many subunits}) \approx C_1 S^{1-\mu} + C_2 S^{q\beta} + \mathcal{O}(S^{\min(1-\mu, q\beta)}). \quad (66)$$

Finally, we have that¹⁹⁹

$$\mathbb{E}[\sigma^q|S] = C_1 S^{1-\mu} + C_2 S^{q\beta} + C_3 S^{\alpha-\mu} + \mathcal{O}(S^{\min(\alpha-\mu, 1-\mu, q\beta)}). \quad (67)$$

The fact that the dominant term is $\propto S^{\alpha-\mu}$, as predicted by the equation above, can also be proven from Equation (48). Consider the term $\int dR R^2 P(R|S)$, which represents the conditional variance of a firm's absolute growth, $\mathbb{V}[R|S]$. We will surmise that $\mathbb{V}[R|S] \propto S^b$ for some b and find the value of b such that this integral scales as $\lambda^{\mu-2}$ as stated in Lemma 5. Doing this substitution in Equation (48) leads, when $b > \alpha$, to¹⁹⁹

$$-\frac{\partial^2 \hat{P}(\lambda, q)}{\partial q^2} \Big|_{q=0} \propto \int_0^\infty dS S^{-(\alpha+1)} S^b \exp(-\lambda S) = \Gamma[b-\alpha] \lambda^{\alpha-b}, \quad (160)$$

which combined with Equation (56) in Lemma 5 implies that²²

$$\lambda^{\mu-2} \propto \lambda^{\alpha-b} \Rightarrow b = \alpha - \mu + 2, \quad (120)$$

which is larger than α when $\mu < 2$. This proves that $\mathbb{V}[R|S] \propto S^{\alpha-\mu+2}$ and gives directly¹⁹⁹

$$\mathbb{E}[\sigma^2|S] = \frac{\mathbb{E}[R^2|S]}{S^2} \propto S^{\alpha-\mu}, \quad (196)$$

as wanted.¹⁹⁹

◻ 196

²⁸Note that for $\alpha = -1$, corresponding to Gabaix' model, Eq. (63) precisely recovers Eq. (5), as it should.¹⁹⁸

A.8. Proof of Proposition 6. 214

Proposition 6. The distribution of growth rates conditional on size S and on growth volatility σ is given, for large S , by: 214

$$P_S(g|\sigma, S) \approx (1 - \pi(S)) \mathcal{N}(0, \sigma^2) + \pi(S) Q_\eta, \quad (68) \quad 204$$

where $\mathcal{N}(0, \sigma^2)$ is a Gaussian distribution with variance $\sigma^2 = \sigma_0^2 H$ and Q_η a non universal distribution that depends on the distribution of the sub-unit growth shocks η . The weight $\pi(S)$ represents the probability of observing a large firm with only few sub-units vanishing when size grows larger as $S^{\alpha-\mu}$. 201

Neglecting large firms with a small number of sub-units and integrating Eq. (12) over the first term of the distribution 204 $P(\sigma|S)$ in Eq. (10) gives 201

$$P(g|S) \sim S^\beta L_{\mu,0}(gS^\beta), \quad \text{when } g \ll 1, \quad (69)$$

where $L_{\mu,0}(\cdot)$ is the symmetric Lévy alpha-stable probability density with stability parameter $1 < \mu < 2$. Because of the cut-off in the distribution of σ , this distribution also has a cut-off, with $P(g|S) = 0$ for $g \gtrsim S$. The complete distribution 201 $P(g)$ is obtained by integrating over $P(s)$, and behaves asymptotically as $P(g) \sim |g|^{-1-\mu}$. 201

Proof. Eq. (12) states simply that, conditional on the size S , a fraction $1 - \pi(S)$ of firms will be such that $S \propto K$ and 202 will be made up of $K \gg 1$ sub-units. These firms will have growth rates that are the sum of $K \gg 1$ sub-unit growth 202 rates, resulting in a Gaussian density of variance σ^2 . The second contribution corresponds to firms with $K = \mathcal{O}(1)$, and 202 therefore the central limit theorem does not apply and the distribution is closer to that of the individual sub-units' growth 202 rates η_{ijt} . 202

Obtaining the distribution of $P(g|S)$ is in principle possible by integrating directly over the volatility σ with its 202 probability distribution $P(\sigma)$ which has been discussed above. We proceed instead by studying the distribution $P(S, R)$ 202 introduced above, finding first the distribution of $R|S$, the absolute size change conditional on size, which will then allow 202 to find the distribution $P(g|S)$. 202

Writing $P(S, R) = P(S)P(R|S)$, using the definitions from (46), we have that 196

$$\widehat{P}(\lambda, q = \theta\lambda^{1/\mu}) = \frac{\int_0^{+\infty} ds}{180} \frac{186}{174} \frac{22}{18} \frac{33}{25} \frac{45}{18} P(S) P(R|S) \exp(i\theta\lambda^{1/\mu} R - \lambda S). \quad (70) \quad 171$$

Next, we surmise that when $P(R|S) = S^{-1/\mu} L_{0,\mu}(RS^{-1/\mu})$, i.e. when $R|S$ is distributed according to a symmetric Lévy 184 distribution with parameter μ , Equation (70) has the same form as that found in Equation (53) of Corollary 3.

Indeed, setting $v = RS^{-1/\mu}$ in (70) we obtain 202

$$\begin{aligned} \widehat{P}(\lambda, q = \theta\lambda^{1/\mu}) &= \frac{\int_0^{+\infty} ds}{180} \frac{78}{18} \frac{70}{25} \frac{274}{18} \frac{33}{25} \frac{45}{18} P(S) \exp(i\theta\lambda^{1/\mu} S^{1/\mu} v - \lambda S) 22 \quad 33 \quad 45 \\ &\equiv \frac{\int_0^{+\infty} dv}{180} \frac{185}{181} \frac{174}{174} P(S) \exp(-\lambda S) \exp(i\theta\lambda^{1/\mu} S^{1/\mu} v) 174 \end{aligned}$$

where one notes that the integral in v is the characteristic function or Fourier transform of a symmetric Lévy alpha Stable 187 distribution of parameter μ , $L_{0,\mu}$, evaluated at $\theta\lambda^{1/\mu} S^{1/\mu}$. This characteristic function behaves as $\int dv e^{itv} \propto \exp(-At^{1/\mu})$, where A is a constant. Applying this to the equation above leads to: 202

$$\widehat{P}(\lambda, q = \theta\lambda^{1/\mu}) = \frac{\int_0^{+\infty} ds}{186} \frac{195}{186} P(S) \exp(-\lambda S) \exp(-A\theta^\mu \lambda S). \quad 193$$

Then 161

$$\begin{aligned} \widehat{P}(\lambda, q = \theta\lambda^{1/\mu}) &= \frac{\int_0^{+\infty} ds}{186} \frac{78}{22} \frac{70}{33} \frac{274}{45} \frac{33}{25} \frac{45}{18} P(S) \exp(i\theta\lambda^{1/\mu} S^{1/\mu} v - \lambda S) 22 \quad 33 \quad 45 \\ &\equiv \frac{\int_0^{+\infty} ds}{186} \frac{78}{22} \frac{70}{33} \frac{74}{45} \frac{22}{25} \frac{33}{18} \frac{45}{64} P(S) \exp(i\theta\lambda^{1/\mu} S^{1/\mu} v) 242 \quad 22 \quad 33 \end{aligned}$$

[the integral in v is the Fourier transform of $L_{0,\mu}$ which has an exponential form] 79 7 12

$$\equiv \frac{\int_0^{+\infty} ds}{187} \frac{78}{188} \frac{70}{188} \frac{74}{187} P(S) \exp(-\lambda S) \exp(-A\theta^\mu \lambda S) 22 \quad 33 \quad 45$$

[where A is a constant] 202

$$\begin{aligned} &\equiv \frac{\int_0^{+\infty} ds}{184} \frac{78}{22} \frac{70}{33} \frac{74}{45} P(S) \exp(-\lambda S(1 + A\theta^\mu)) 22 \quad 33 \quad 45 \\ &= 1 - \frac{\int_0^{+\infty} ds}{184} \frac{185}{185} P(S) (1 - \exp(-\lambda S(1 + A\theta^\mu))) 174 \end{aligned}$$

[using twice the linear approximation of $-e^{-x} \sim x - 1$]

$$\begin{aligned} &= 1 - \lambda \mathbb{E}[S] - A\theta^\mu \lambda \mathbb{E}[S] + \mathcal{O}(\lambda) \quad 194 \\ &= 1 - \lambda \mathbb{E}[S] (1 + A\theta^\mu) + \mathcal{O}(\lambda) \quad 194 \end{aligned}$$

which indeed matches Equation (53). 202

Now, this proves that $RS^{-1/\mu}$ is distributed according to a Lévy distribution with parameter μ , and therefore 202

$$P(R|S) \sim S^{-1/\mu} L_{\mu,0}(RS^{-1/\mu}). \quad (71) \quad 202$$

since $R = qS$ and since $\beta = 1 - 1/\mu$, this proves the first part of the proposition. The cut-off value at $q \sim 1$ results from 202
the fact that the Herfindahl has a cut off at $H = 1$. 202

For the second part, we first write that $P(g) = \int dS P(S)P(g|S)$, and then consider the cumulative density function, 202
 $P_>(g) := \int_g^\infty dS P(g|S)$. This yields 200

$$\begin{aligned} P_>(g) &= \int_g^\infty \frac{dS}{22} \frac{22}{22} \frac{33}{33} \frac{45}{45} L_{0,\mu}(g_1 S^\beta) \quad 22 \quad 33 \quad 45 \\ &\stackrel{\text{using } 74}{=} \int_g^\infty dS P(S) S^\beta \int_{g_1}^\infty dS L_{0,\mu}(g_1 S^\beta) \quad 51 \\ &\stackrel{\text{(using that asymptotically, } L_{0,\mu}(x) \sim x^{-1-\mu})}{=} \int_g^\infty dS P(S) S^\beta S^{-\beta(1+\mu)} \int_{g_1}^\infty dS \frac{1}{22} \frac{33}{33} \frac{45}{45} \quad 161 \quad 242 \quad 22 \\ &\stackrel{\text{using } 74}{=} \int_g^\infty dS P(S) S^{-\beta\mu} \quad 51 \\ &\sim g^{-\mu} \end{aligned} \quad (72) \quad 202$$

where we have used the fact that $\beta\mu = \mu - 1 < 1$ so that the integral over S is convergent for both small and large S . 202
This shows that $P(g)$ is a mixture of Lévy alpha-stable distributions with a power-law tail with exponent μ . 202

■ 196

A.9. Proof of Proposition 7 203

Proposition 7. *Proposition 3, 4, 5 and 6 are robust against the additive aggregation of firms into (possibly fictitious) 204
supra-firms.* 204

Proof. Consider two firms, i and j , with K_i and K_j sub-units respectively. Since both are Pareto distributed with 205
exponent α , the additive aggregation of these two firms produces a new entity with $K_i + K_j$ sub-units, which is also 205
asymptotically Pareto with the same exponent α . The size distribution of the sub-units clearly remains Pareto distributed 205
as well. As a consequence, starting with N firms which are then merged into N/n “super-firms” leads to the same 205
statistical properties for size, growth and the size/growth-volatility relationship discussed above. ■ 205

B. Descriptive statistics and further investigations

B.1. Main sample

In this Appendix we report descriptive statistics on size (\bar{S}), normalized size (S) and on their (log) growth rates for the main sample used in the paper. We also discuss the existence of the hump $H(\sigma)$ predicted by Proposition 4 and explore the consequences of using the standard deviation to proxy for volatility.

Descriptive statistics. In Table 2 statistics are reported at the firm-year level. This sample contains more than 1.2 millions of firm-year observations, with an extreme range of variation both for sizes and growth rates and for the three variants (nominal, deflated and normalized). As expected different variants of growth rates do not differ much and, less expected, their range of variation is well centered around zero.

Table 2: Descriptive statistics on size and growth rates (main sample)

	N	Mean	St. Dev.	Min	Max	212
size \bar{S}	1,228,260	348,088,528.000	2,050,671,382.000	1,000,000	152,079,000,000.000	210
size S deflated	1,228,260	481,340,797.000	2,427,441,597.000	940,955	147,203,757,866.000	210
size S	1,228,260	1.001	4.734	0.00000	279.152	210
growth rate \bar{q}	1,121,115	0.094	0.591	-12.324	12.435	210
growth rate \bar{q} deflated	1,121,115	0.066	0.590	-12.386	12.403	210
growth rate q	1,121,115	0.045	0.593	-12.070	12.318	210

Notes: Growth rates are computed as logarithmic differences. Data source: Compustat.

Table 3 reports statistics at the firm level. In this sample there are 24,233 different firms. Each firm has on average 46 growth rates whose volatility, proxied by the corresponding Mean Absolute Deviation (mad) adjusted by $\sqrt{\pi/2}$, ranges from 0.002 to 5.9 with an average of 0.48.

Table 3: Descriptive statistics on size and growth volatility (main sample)

	N	Mean	St. Dev.	Min	Max	217
size S	24,233	0.484	2.466	0.00000	109.177	113 22 33
num growth rates	24,233	46,264	44,972	2	236	22 33 45
growth volatility (mad)	24,233	0.479	0.490	0.002	5.879	242 22 33
growth volatility (sd)	24,233	0.532	0.525	0.002	5.753	22 33 45

Notes: “mad” and “sd” represent the mean absolute deviation adjusted by the factor $\sqrt{\pi/2}$ and the standard deviation. Data source: Compustat.

Table 4 reports statistics for normalized growth rates \bar{q} grouped in the 25 size bins built on the average normalized size \bar{S}_i . By construction each bin contains the same number of firms, but a significantly different number of observations increasing with size. Looking at the range of variation we observe few extreme realizations which we have checked do not drive our main results.

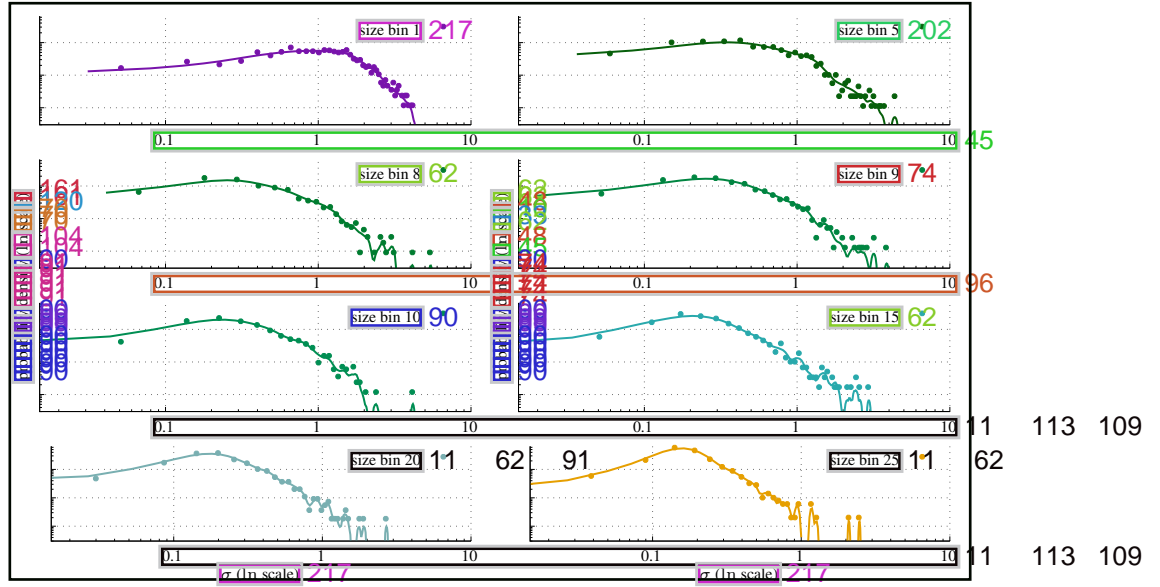
Table 4: Rescaled growth rates by size bin (main sample)

bin	n firms	n obs.	n distinct obs.	mean	median	sd	min	max	212
1	956	15,429	15,162	0.035	-0.023	5.395	-122.467	612.003	120
2	956	22,036	21,884	-0.051	-0.034	8.903	-1,298.563	88.184	120
3	956	25,541	25,474	0.0004	-0.021	1.707	-122.556	39.474	120
4	956	29,843	29,797	-0.002	-0.033	1.482	-46.430	46.910	120
5	956	31,695	31,675	-0.009	-0.016	1.534	-76.348	33.811	120
6	956	33,059	33,041	-0.030	-0.016	3.681	-605.375	47.771	120
7	956	35,286	35,271	-0.025	-0.011	2.678	-408.559	59.716	120
8	956	35,422	35,395	-0.005	-0.010	1.903	-51.151	174.698	120
9	956	36,899	36,882	-0.044	-0.005	4.616	-748.208	30.829	120
10	955	37,570	37,559	-0.019	-0.014	1.490	-37.562	22.549	120
11	955	36,489	36,464	-0.027	-0.004	1.609	-79.893	19.165	120
12	955	38,315	38,306	-0.022	-0.003	2.161	-124.045	259.869	120
13	955	38,322	38,319	-0.020	-0.018	1.781	-176.321	50.916	120
14	955	40,349	40,340	-0.028	-0.039	2.244	-309.692	35.023	120
15	955	40,532	40,529	-0.019	-0.024	5.150	-674.556	721.555	120
16	955	43,893	43,891	-0.009	-0.032	1.609	-59.192	125.763	120
17	955	43,855	43,839	-0.013	-0.037	1.631	-148.291	63.491	120
18	955	46,803	46,801	-0.008	-0.048	1.460	-94.761	26.068	120
19	955	50,316	50,310	-0.008	-0.045	1.370	-51.656	20.239	120
20	955	55,136	55,133	-0.009	-0.054	1.503	-137.243	59.857	120
21	955	57,689	57,674	-0.005	-0.068	1.464	-96.574	66.960	120
22	955	63,666	63,661	-0.010	-0.060	1.798	-222.718	145.668	120
23	955	74,665	74,649	-0.003	-0.060	1.327	-57.865	26.530	120
24	955	83,288	83,285	-0.004	-0.083	1.460	-83.315	99.560	120
25	955	104,316	104,313	-0.047	-0.093	14.293	-4,593.166	18.729	120

Notes: Descriptive statistics of heterogeneously rescaled growth rates \hat{q} binned according to their average size \bar{S} . Data source: Compustat.

Missing hump in $H(\sigma)$. Figure 8 reports, on a double log scale, the distributions of the growth rate volatility for various size bins. We see no sign of an hump for large volatilities and we confirm visual inspection with the non-parametric test of bi-modality presented in Ameijeiras-Alonso et al. (2019) which rejects the existence of a second mode at any reasonable level of statistical significance for all bins. Together with bin 1, 5, 10, 15, 20 and 25 we report bin 8 and 9 associated with the lower p-value for the null hypothesis that the true number of modes is 1. 215

Figure 8: Growth volatility distribution by size bin (main sample) 218



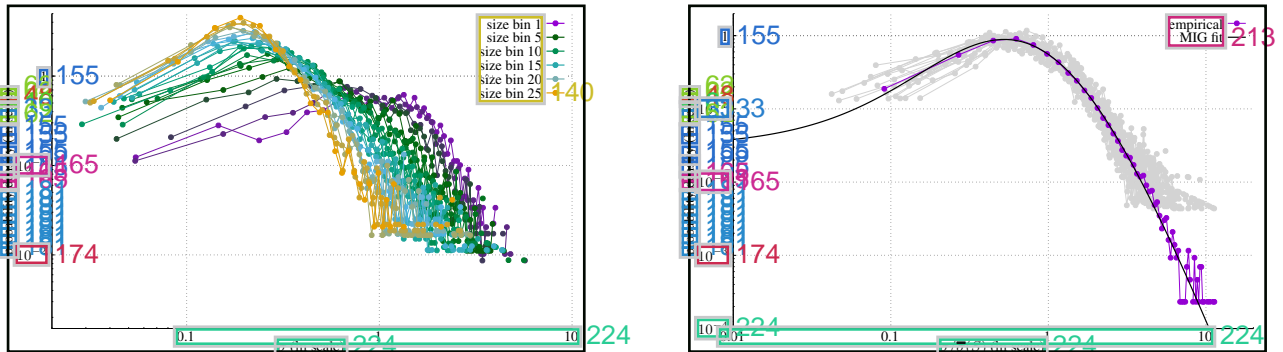
Notes. Panels report for different bins defined in term of normalized size, the distribution of the growth rate volatility on a double log scale. Points represent the histogram while solid lines the kernel density estimates. In all the figures volatility is computed as the mean absolute deviation multiplied by the factor $\sqrt{\pi}/2$. Data source: Compustat. 220

Table 5: ACR non parametric test of bi-modality for the growth volatility distribution 241

bin	ACR statistic	p.value	n	bin	ACR statistic	p.value	n	bin	ACR statistic	p.value	n
1	0.013	0.944	970	11	0.013	0.784	969	21	0.016	0.016	0.016
2	0.015	0.66	970	12	0.016	0.34	969	22	0.015	0.015	0.015
3	0.014	0.684	970	13	0.013	0.846	969	23	0.017	0.017	0.017
4	0.017	0.247	970	14	0.014	0.689	969	24	0.016	0.016	0.016
5	0.013	0.786	970	15	0.017	0.2	969	25	0.011	0.011	0.011
6	0.014	0.7	970	16	0.013	0.799	969	224			
7	0.013	0.737	970	17	0.012	0.977	969	224			
8	0.02	0.082	970	18	0.014	0.635	969	224			
9	0.02	0.069	969	19	0.017	0.253	969	224			
10	0.012	0.961	969	20	0.018	0.222	969	224			

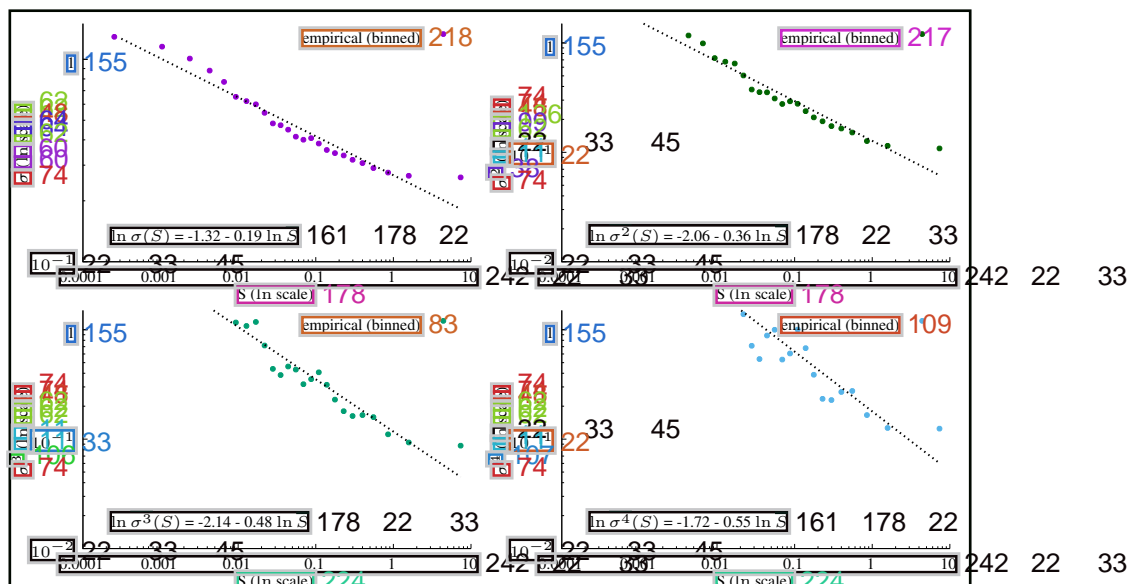
Growth volatility estimated using the standard deviation. Figure 9 and Figure 10 report the key empirical results on growth volatility when we replace the mean absolute deviation (mad) with the standard deviation (sd). The shape of its distribution, its scaling with size and the quantitative fit of the Modified Inverse Gamma distribution (MIG) remain qualitatively the same. 218

Figure 9: Growth volatility distribution (volatility is computed as standard deviation) 219



Notes. Left panel reports on a double log scale and for 25 bins, defined in term of normalized size, the distribution of the growth rate volatility. Right panel reports on a double log scale the distribution of the growth volatility rescaled by the average volatility observed in each bin together with an Inverse Gamma fit (solid line). The ML estimates of the scale, shape and location parameter are 4.922(0.147), 4.668(0.089), and 0.344(0.010) respectively. In all the figures volatility is computed as the standard deviation. Data source: Compustat. 216

Figure 10: Size and growth volatility (volatility is computed as standard deviation) 220



Notes. The four panels report on a double log scale the binned relation between normalized size and the first four sample moments of growth volatility together with an OLS linear fit. In all panel the number of bins is set to 25 and volatility is computed as the standard deviation. Data source: Compustat. 220

B.2. Sample with firms with 20 or more growth rates 221

In this Appendix to alleviate concerns associated with measurement errors in estimating growth volatilities we change the sample and consider firms with 20 or more growth rates only. 222

Descriptive statistics. Table 6 reports statistics at the firm-year level. The overall picture remains very similar to that reported for the main sample. 223

Table 6: Descriptive statistics on size and growth rates (firms with 20 or more growth rates) 242 22 33

	N	Mean	St. Dev.	Min	Max	224
size \bar{S}	1,103,590	379,856,536.000	2,155,729,951.000	1,000,000	152,079,000,000.000	226
size \bar{S} deflated	1,103,590	525,526,423.000	2,548,717,299.000	940,955	147,203,757,866.000	224
size S	1,103,590	1.000	4.528	0.00000	245,280	224
growth rate \bar{q}	1,032,199	0.087	0.543	-12.324	12,435	224
growth rate \bar{q} deflated	1,032,199	0.058	0.543	-12.386	12,403	224
growth rate q	1,032,199	0.037	0.545	-12.123	12,313	224

Notes: Growth rates are computed as logarithmic differences. Data source: Compustat. 228

Table 7 reports statistics firm level. In this sample the number of firms reduces to 15,788 but, a part of that, growth rates display statistical properties similar to those observed in the main sample. 225

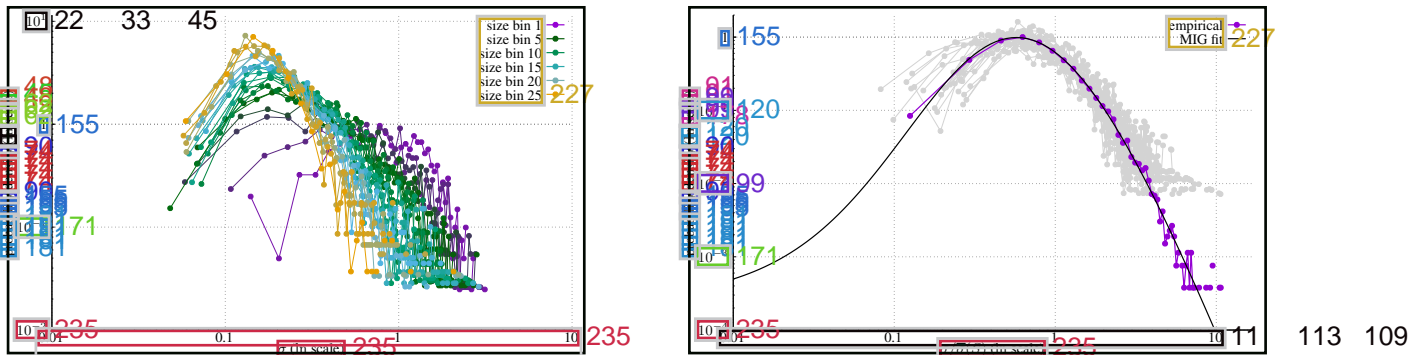
Table 7: Descriptive statistics on size and growth volatility (firms with 20 or more growth rates) 224

	N	Mean	St. Dev.	Min	Max	224
size S	15,788	0.573	2.502	0.00001	100,663	113 22 33
num growth rates	15,788	65.379	45.192	20	236	22 33 45
growth volatility (mad)	15,788	0.399	0.367	0.022	3.171	242 22 33
growth volatility (sd)	15,788	0.458	0.421	0.028	3.459	242 22 33

Notes: "mad" and "sd" represent the mean absolute deviation adjusted by the factor $\sqrt{\pi/2}$ and the standard deviation. Data source: Compustat. 113 7 83

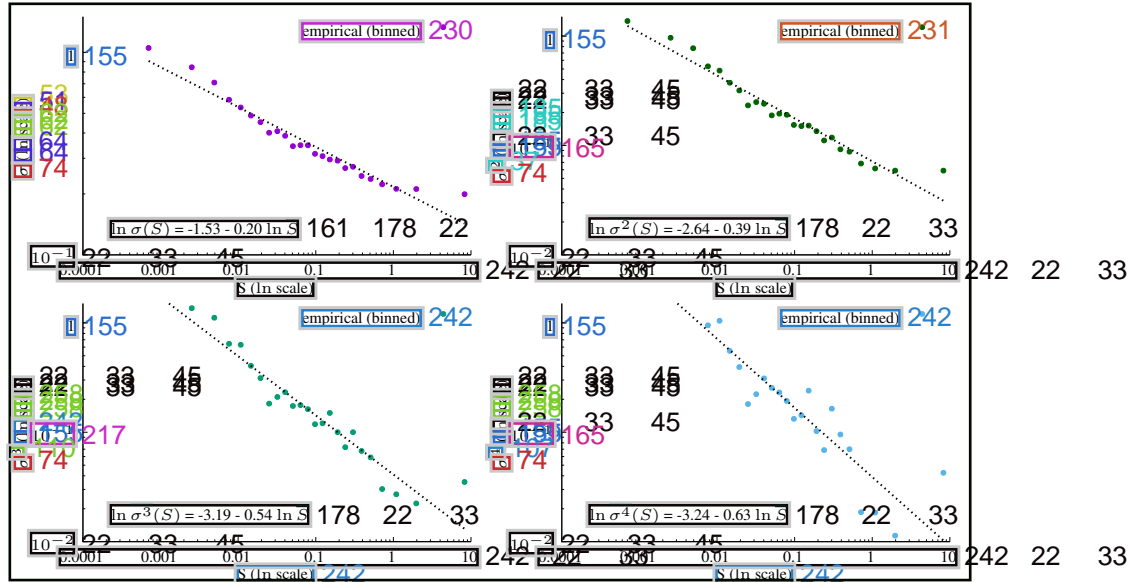
Growth volatility. Figure 11 and Figure 12 report the key empirical results on growth volatility. The shape of its distribution, its scaling with size and the quantitative fit of the Modified Inverse Gamma distribution (MIG) remain qualitatively the same as in the main sample. 227

Figure 11: Growth volatility distribution (firms with 20 or more growth rates) 228



Notes. Left panel reports on a double log scale and for 25 bins, defined in term of normalized size, the distribution of the growth rate volatility. Right panel reports on a double log scale the distribution of the growth volatility rescaled by the average volatility observed in each bin together with an Inverse Gamma fit (solid line). The ML estimates of the scale, shape and location parameter are 4.381(0.151), 4.638(0.104), and 0.204(0.010), respectively. In all the figures volatility is computed as the mean absolute deviation multiplied by the factor $\sqrt{\pi/2}$. Data source: Compustat. 228

Figure 12: Size and growth volatility (firms with 20 or more growth rates) 229



Notes. The four panels report on a double log scale the binned relation between normalized size and the first four sample moments of growth volatility together with an OLS linear fit. In all panel the number of bins is set to 25 and volatility is computed as the mean absolute deviation multiplied by the factor $\sqrt{\pi/2}$. Data source: Compustat.

GSE fit on rescaled growth rates. Table 8 reports the GSE estimates for this sample. The main message discussed in the paper looks qualitatively unaffected by this change in the sample selection criterion. 229 230

Table 8: Symmetric GSE fit (firms with 20 or more growth rates) 243

	C	u	v	w	z	Prob. mass	$ w, w $	237
Whole sample	91	11	22					
homogeneous rescaling	0.75 (0.003)	0.452 (0.002)	0.012 (0.000)	0.715 (0.004)	0.413 (0.001)	0.699	22	33
heterogeneous rescaling	0.503 (0.002)	0.846 (0.004)	0.024 (0.001)	1.728 (0.013)	0.417 (0.003)	0.895	242	22
Size bin	11	62						
1	0.452 (0.010)	0.872 (0.026)	0.05 (0.003)	1.505 (0.097)	0.681 (0.015)	0.84	11	22
2	0.508 (0.017)	0.659 (0.036)	0.04 (0.003)	0.85 (0.093)	0.734 (0.014)	0.653	11	22
3	0.426 (0.006)	1.086 (0.011)	0.043 (0.002)	2.754 (0.051)	0.194 (0.012)	0.963	11	22
4	0.528 (0.012)	0.706 (0.021)	0.001 (0.002)	1.116 (0.062)	0.611 (0.010)	0.76	11	22
5	0.495 (0.007)	0.875 (0.011)	0.022 (0.002)	1.855 (0.040)	0.375 (0.008)	0.906	11	22
6	0.481 (0.006)	0.926 (0.010)	0.017 (0.002)	2.069 (0.040)	0.346 (0.008)	0.928	11	22
7	0.508 (0.008)	0.848 (0.012)	-0.009 (0.002)	1.77 (0.045)	0.378 (0.009)	0.9	11	22
8	0.477 (0.009)	0.952 (0.015)	0.026 (0.003)	2.226 (0.060)	0.285 (0.013)	0.941	11	22
9	0.499 (0.009)	0.851 (0.014)	-0.003 (0.002)	1.719 (0.053)	0.451 (0.010)	0.892	11	22
10	0.498 (0.018)	0.849 (0.031)	-0.021 (0.004)	1.69 (0.118)	0.503 (0.021)	0.889	11	22
11	0.472 (0.008)	0.93 (0.014)	-0.029 (0.002)	2.045 (0.057)	0.389 (0.011)	0.926	11	22
12	0.506 (0.011)	0.82 (0.019)	0.002 (0.003)	1.574 (0.067)	0.503 (0.012)	0.87	11	22
13	0.456 (0.010)	1.004 (0.017)	-0.034 (0.003)	2.426 (0.073)	0.261 (0.017)	0.952	11	22
14	0.47 (0.006)	0.982 (0.010)	0.011 (0.002)	2.376 (0.041)	0.259 (0.009)	0.951	11	22
15	0.479 (0.008)	0.946 (0.013)	0.02 (0.002)	2.174 (0.053)	0.333 (0.011)	0.939	11	22
16	0.481 (0.009)	0.925 (0.015)	-0.003 (0.002)	2.069 (0.061)	0.355 (0.013)	0.93	11	22
17	0.488 (0.010)	0.892 (0.017)	-0.016 (0.003)	1.914 (0.065)	0.391 (0.013)	0.917	11	22
18	0.508 (0.009)	0.828 (0.014)	0.022 (0.002)	1.649 (0.051)	0.448 (0.010)	0.889	11	22
19	0.485 (0.009)	0.917 (0.014)	0.03 (0.002)	2.064 (0.053)	0.314 (0.011)	0.929	11	22
20	0.518 (0.011)	0.798 (0.017)	0.043 (0.002)	1.548 (0.057)	0.451 (0.011)	0.872	11	22
21	0.54 (0.012)	0.709 (0.018)	0.028 (0.002)	1.192 (0.055)	0.553 (0.009)	0.793	11	22
22	0.513 (0.009)	0.825 (0.013)	0.022 (0.002)	1.679 (0.045)	0.41 (0.009)	0.893	11	22
23	0.547 (0.019)	0.667 (0.028)	0.001 (0.003)	1.037 (0.080)	0.601 (0.013)	0.751	11	22
24	0.506 (0.010)	0.79 (0.015)	0.078 (0.002)	1.502 (0.050)	0.449 (0.009)	0.867	11	22
25	0.534 (0.011)	0.728 (0.015)	0.072 (0.002)	1.313 (0.046)	0.47 (0.008)	0.836	11	22
Time window	237							
2 years	0.454 (0.003)	1.044 (0.006)	0.007 (0.001)	2.671 (0.029)	0.309 (0.006)	0.97	235	
3 years	0.449 (0.003)	1.11 (0.005)	0.004 (0.001)	3.189 (0.028)	0.208 (0.007)	0.988	235	
4 years	0.444 (0.004)	1.164 (0.006)	-0.005 (0.001)	3.658 (0.031)	0.037 (0.009)	0.993	235	

Notes: estimates are obtained with a non linear least square algorithm applied to kernel density estimates evaluated on a regular grid in the interval $[-8, 8]$. This procedure is applied to homogeneously rescaled growth rates, and heterogeneously rescaled growth rates in different size bins and computed over different time windows. Data source: Compustat.

B.3. Sample with firms whose fiscal year ends in December 232

In this Appendix we explore if the presence in the sample of firms with asynchronous fiscal years affects our results. To this aim we change the sample and consider firms whose fiscal year ends in December only. 233

Descriptive statistics. Table 9 reports statistics at the firm-year level. The overall picture remains very similar to 234 that reported for the main sample. 234

Table 9: Descriptive statistics on size and growth rates (firms whose fiscal year ends in December) 235

	N	Mean	St. Dev.	Min	Max
size \bar{S}	717,545	431,790,843.000	2,135,254,603.000	1,000.000	132,872,000,000.000
size \bar{S} deflated	717,545	600,634,668.000	2,605,466,179.000	940.955	147,203,757,866.000
size S	717,545	1.089	4.632	0.00000	215,495
growth rate \bar{q}	670,165	0.089	0.543	-12,324	12,435
growth rate \bar{q} deflated	670,165	0.061	0.543	-12,386	12,403
growth rate q	668,705	0.047	0.543	-12,224	12,328

Notes: Growth rates are computed as logarithmic differences. Data source: Compustat. 239

Table 10 reports statistics firm level. In this sample the number of firms reduces to 10,974 but, a part of that, growth rates display statistical properties similar to those observed in the main sample. 236

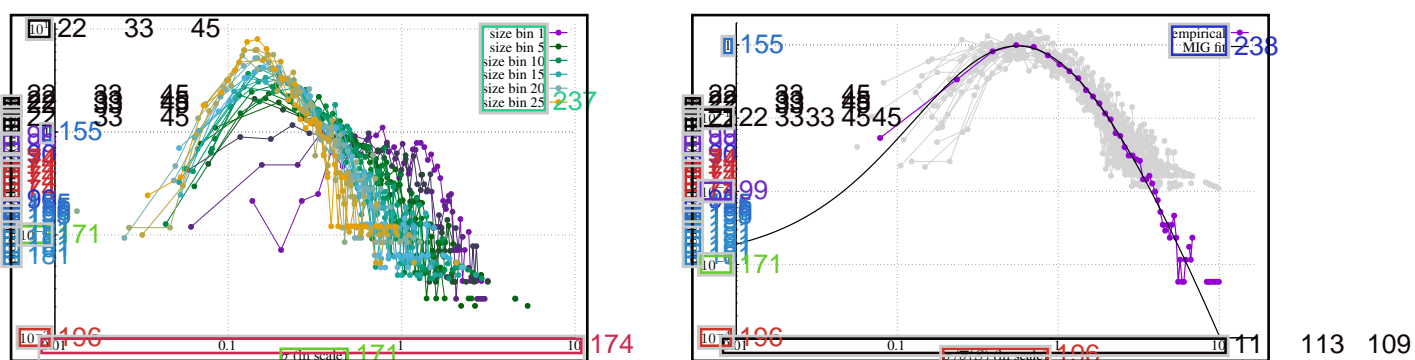
Table 10: Descriptive statistics on size and growth volatility (firms whose fiscal year ends in December) 237

	N	Mean	St. Dev.	Min	Max	237
size S	10,974	0.622	2.591	0.00001	94.560	113 22 33
num growth rates	10,974	60.935	45.060	2	233	22 33 45
growth volatility (mad)	10,974	0.395	0.382	0.000	5.380	22 33 45
growth volatility (sd)	10,974	0.453	0.433	0.000	5.168	22 33 45

[Notes: "mad" and "sd" represent the mean absolute deviation adjusted by the factor $\sqrt{\pi/2}$.] 113 7 83
and the standard deviation. Data source: Compustat.

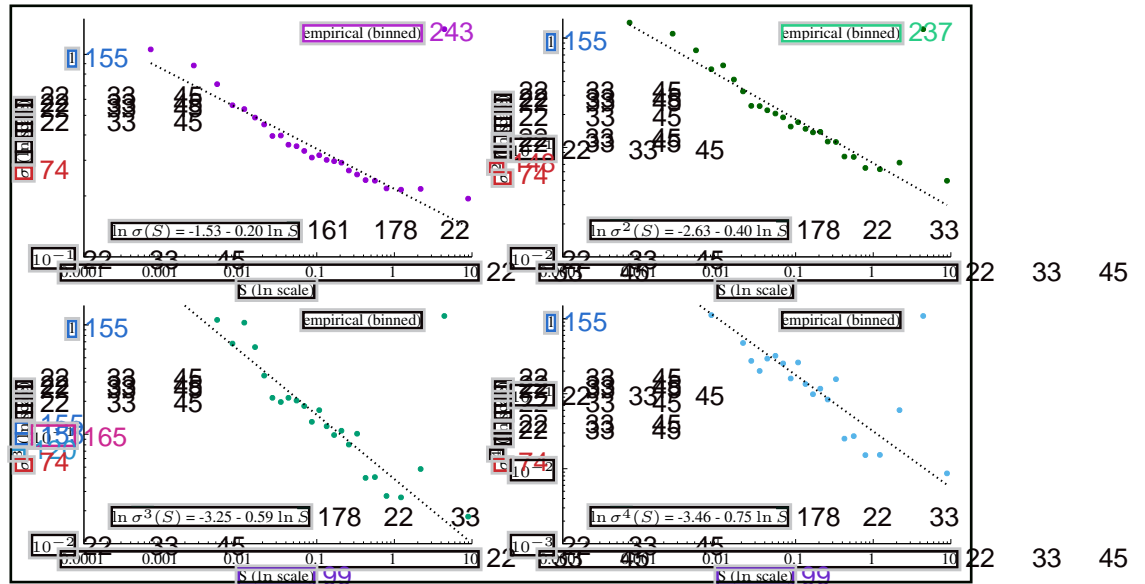
Growth volatility. Figure 13 and Figure 14 report the key empirical results on growth volatility. The shape of its distribution, its scaling with size and the quantitative fit of the Modified Inverse Gamma distribution (MIG) remain qualitatively the same as in the main sample.¹²³⁸

Figure 13: Growth volatility distribution (firms whose fiscal year ends in December) 239



Notes. Left panel reports on a double log scale and for 25 bins, defined in term of normalized size, the distribution of the growth rate volatility. Right panel reports on a double log scale the distribution of the growth volatility rescaled by the average volatility observed in each bin together with an Inverse Gamma fit (solid line). The ML estimates of the scale, shape and location parameter are 1.330(0.174), 1.510(0.110) and 0.225(0.019), respectively. In all the figures volatility is computed as the mean absolute deviation multiplied by the factor $\sqrt{\pi/2}$. Data source: Compustat. 198

Figure 14: Size and growth volatility (only firms with end of fiscal year in December) [240]



Notes. The four panels report on a double log scale the binned relation between normalized size and the first four sample moments of growth volatility together with an OLS linear fit. In all panel the number of bins is set to 25 and volatility is computed as the mean absolute deviation multiplied by the factor $\sqrt{\pi}/2$. Data source: Compustat. [191]

GSE fit on rescaled growth rates. Table 11 reports the GSE estimates for this sample. The main message discussed in the paper looks qualitatively unaffected by this change in the sample selection criterion. [241]

Table 11: Symmetric GSE fit [235]

	C	u	v	w	z	Prob. mass $ w, w $	235
<i>Whole sample</i>	91	11	22				
homogeneous rescaling	0.768 (0.004)	0.431 (0.002)	0.015 (0.000)	0.67 (0.005)	0.416 (0.001)	0.685	22 33 45
heterogeneous rescaling	0.512 (0.003)	0.819 (0.005)	0.027 (0.001)	1.629 (0.017)	0.43 (0.003)	0.882	22 33 45
<i>Size bin</i>	11	62					
1	0.398 (0.012)	1.111 (0.035)	0.05 (0.004)	2.594 (0.182)	0.53 (0.031)	0.954	11 22 33
2	0.51 (0.020)	0.632 (0.044)	0.043 (0.004)	0.762 (0.105)	0.757 (0.015)	0.612	11 22 33
3	0.441 (0.007)	1.028 (0.013)	0.037 (0.002)	2.447 (0.056)	0.291 (0.012)	0.947	11 22 33
4	0.519 (0.014)	0.755 (0.023)	-0.03 (0.003)	1.324 (0.072)	0.531 (0.013)	0.818	11 22 33
5	0.494 (0.009)	0.874 (0.014)	0.001 (0.002)	1.829 (0.052)	0.411 (0.010)	0.903	11 22 33
6	0.511 (0.010)	0.836 (0.015)	-0.003 (0.002)	1.716 (0.055)	0.398 (0.011)	0.892	11 22 33
7	0.502 (0.012)	0.895 (0.016)	0.032 (0.003)	2.036 (0.062)	0.274 (0.014)	0.927	11 22 33
8	0.489 (0.012)	0.892 (0.019)	-0.001 (0.003)	1.907 (0.074)	0.406 (0.014)	0.915	11 22 33
9	0.475 (0.009)	0.952 (0.014)	0.01 (0.002)	2.206 (0.058)	0.31 (0.012)	0.939	11 22 33
10	0.479 (0.011)	0.95 (0.018)	-0.016 (0.003)	2.204 (0.078)	0.37 (0.016)	0.945	11 22 33
11	0.486 (0.009)	0.892 (0.016)	0.008 (0.002)	1.888 (0.060)	0.417 (0.012)	0.913	11 22 33
12	0.473 (0.020)	0.868 (0.037)	-0.07 (0.005)	1.713 (0.139)	0.504 (0.025)	0.892	11 22 33
13	0.466 (0.010)	1.006 (0.016)	0.011 (0.003)	2.521 (0.068)	0.197 (0.016)	0.957	11 22 33
14	0.454 (0.011)	1.025 (0.019)	0.025 (0.004)	2.579 (0.082)	0.211 (0.019)	0.958	11 22 33
15	0.47 (0.011)	0.972 (0.018)	0.001 (0.003)	2.312 (0.074)	0.266 (0.016)	0.945	11 22 33
16	0.483 (0.011)	0.923 (0.018)	0.009 (0.003)	2.077 (0.070)	0.331 (0.015)	0.93	11 22 33
17	0.557 (0.025)	0.595 (0.039)	-0.012 (0.004)	0.795 (0.094)	0.663 (0.015)	0.631	11 22 33
18	0.496 (0.009)	0.878 (0.014)	0.033 (0.002)	1.886 (0.050)	0.356 (0.010)	0.912	11 22 33
19	0.501 (0.013)	0.842 (0.021)	0.048 (0.003)	1.693 (0.076)	0.441 (0.014)	0.89	11 22 33
20	0.534 (0.014)	0.714 (0.021)	0.051 (0.003)	1.207 (0.064)	0.544 (0.011)	0.8	11 22 33
21	0.533 (0.014)	0.726 (0.020)	0.052 (0.003)	1.259 (0.063)	0.535 (0.011)	0.815	11 22 33
22	0.558 (0.017)	0.671 (0.023)	0.013 (0.003)	1.1 (0.065)	0.54 (0.011)	0.773	11 22 33
23	0.548 (0.018)	0.654 (0.028)	0.041 (0.003)	0.995 (0.077)	0.605 (0.013)	0.739	11 22 33
24	0.515 (0.009)	0.793 (0.013)	0.068 (0.002)	1.566 (0.042)	0.391 (0.008)	0.876	11 22 33
25	0.538 (0.013)	0.732 (0.017)	0.058 (0.003)	1.347 (0.054)	0.451 (0.010)	0.843	11 22 33
<i>Time window</i>	22	33	45				
2 years	0.451 (0.004)	1.055 (0.007)	-0.006 (0.001)	2.736 (0.032)	0.276 (0.007)	0.972	11 22 33
3 years	0.447 (0.004)	1.117 (0.006)	-0.017 (0.001)	3.237 (0.032)	0.172 (0.008)	0.988	11 22 33
4 years	0.45 (0.004)	1.149 (0.006)	-0.019 (0.001)	3.571 (0.030)	0.034 (0.009)	0.993	11 22 33
<i>Notes:</i>	estimates are obtained with a non linear least square algorithm applied to kernel density estimates evaluated on a regular grid in the interval $[-8, 8]$						
This procedure is applied to homogeneously rescaled growth rates, and heterogeneously rescaled growth rates in different size bins and computed over different time windows. Data source: Compustat.	22	33	45	10	22	33	113